Mon. Not. R. Astron. Soc. **355,** 485–503 (2004) doi:10.1111/j.1365-2966.2004.08335.x

The *Hubble Deep Field* North SCUBA Super-map – II. Multiwavelength properties

Colin Borys,[1]★ Douglas Scott,[2] Scott Chapman,[1] Mark Halpern,[2] Kirpal Nandra[3] and Alexandra Pope[2]

[1]*California Institute of Technology, Pasadena, CA 91125, USA*
[2]*Department of Physics & Astronomy, University of British Columbia, Vancouver, BC, V6T 1Z1, Canada*
[3]*Astrophysics Group, Imperial College London, Blackett Laboratory, Prince Consort Road, London SW7 2AZ*

Accepted 2004 August 18. Received 2004 July 25; in original form 2004 April 27

ABSTRACT

We present radio, optical and X-ray-detected counterparts to the submillimetre sources found using SCUBA in the *Hubble Deep Field* North region (GOODS-N). A new counterpart identification statistic is developed to identify properties of galaxies detected at other wavelengths that can be used to aid counterpart identification. We discriminate between criteria that can use used to pre-select submillimetre bright objects, and those that identify the counterpart to a known submillimetre object. Optically faint galaxies detected in the deepest 1.4-GHz radio continuum maps are the only effective way of pre-selecting SCUBA galaxies, and radio sources are the best way to identify counterparts to known submillimetre detections. Looking at radio spectral indices, only the steeper sources (indicative of star formation) are detected in the submillimetre range. Although we find several X-ray identifications, we show that deep *Chandra* images do not contribute to counterpart identifications, as in all cases they are already detected in the more easily obtained VLA radio maps. We also find no evidence for clustering between *Chandra* and SCUBA sources in this field. For a known SCUBA position, the reddest source tends to be the correct association, although we can find no cut on colour, magnitude or clustering property that efficiently pre-selects for SCUBA sources. 15-μm *ISO* sources are statistically detected by SCUBA, but the limiting mid-infrared flux is not low enough to provide useful constraints. We present postage stamp strips for each SCUBA detection in separate bands from X-ray to radio bands, providing direct visual evidence that approximately half of the submillimetre sources in this field remain unidentified, despite an abundance of deep multiwavelength data.

Key words: methods: numerical – methods: statistical – galaxies: formation – galaxies: starburst – infrared: galaxies.

1 INTRODUCTION

Finding distant infrared (IR) luminous galaxies is now a routine occurrence for the Submillimetre Common User Bolometer Array (SCUBA, Holland et al. 1999) on the James Clerk Maxwell Telescope (see Blain et al. 2002). Specifically, we estimate that there have been about 300 published detections in the first 5 yr since the instrument was commissioned in 1997. Much more challenging is determining *what* the galaxies are. To obtain a complete picture it is necessary to compare the submillimetre sources against data obtained at other wavelengths, but this is often quite difficult for a number of reasons. First, the very dust responsible for the strong IR emission obscures and re-processes light at other wavelengths, making the objects more difficult to detect. Secondly, the negative *K*-correction in the submillimetre range that allows an almost distance-independent ability to detect these galaxies does not apply in the optical and radio bands. The most serious issue, however, is the large beam-size in submillimetre surveys; often there are several sources within the SCUBA beam detected at other wavelengths, and without some means to discriminate among them, it is uncertain which (if any) of the sources is the host of the far-IR emission.

Until the advent of the next generation of submillimetre interferometers (particularly ALMA), there is not much that can be done to significantly improve the resolution of the images. However, we can address the other issues by obtaining very deep images of SCUBA fields at other wavelengths in order to better identify faint counterparts. The *Hubble Deep Field* North (HDF-N) (Williams et al. 1996;

★E-mail: borys@caltech.edu

Ferguson, Dickinson & Williams 2000) and its flanking fields, with its wide range of deep imaging across many wavebands, is arguably the best region to use for this purpose.

In this paper, we use this rich multiwavelength data set to determine counterparts to the SCUBA-detected sources in a roughly 0.05 deg^2 region centred on the HDF-N, as described in Borys et al. (2003, hereafter called Paper I) Given the volume of data still being obtained in the region due to the Great Observatories Origins Deep Survey (GOODS) programme, we choose to include only data published or obtained prior to the deep ACS images released in 2003 August. A larger submillimetre map of the HDF-N, and the study of other GOODS data is reserved for future work.

2 REVIEW OF THE HDF-N SUBMILLIMETRE MAPS

Submillimetre maps of the HDF-N were obtained using the SCUBA camera at the James Clerk Maxwell Telescope, including more than 60 shifts of telescope time. We combined the various data sets into a single map, which we refer to as the Super-map. Combining this with detailed simulations allowed us to extract and assess the reliability of the sources. The full data reduction and source extraction algorithm are described in Paper I.

In summary, the Super-map contains 19 sources which were detected at 850 μm with a signal-to-noise ratio (SNR) > 4. An additional list of 15 sources was presented between 3.5 and 4σ. Monte Carlo simulations of the data suggest that the 4σ catalogue should have at most one false detection, but that the number of spurious sources rises drastically for lower thresholds. Thus the 3.5–4σ catalogue is considered less reliable, although we later argue that at least a third are real. The reality of the five sources detected at 450 μm is much less secure, however, as none were found coincident with a source at 850 μm.

Subsets of the data used here have been published by other groups, and in Paper I we compared them against our map, finding no serious discrepancies. However, a new survey by Wang, Cowie & Barger (2004) appeared after this work was submitted which takes a more critical view of other SCUBA analyses of the HDF-N. In Appendix B we compare our results with theirs, and find that in fact their results support the work here and in previous publications.

3 STATISTICAL CRITERIA FOR FINDING COUNTERPARTS

To identify the most likely counterparts for our SCUBA detections, we need first to choose a method for associating counterparts. As the Super-map has non-uniform noise, our catalogue includes sources at a variety of signal and SNR levels (including some faint high SNR sources, as well as brighter low-SNR sources). Because of the variable effects of pointing uncertainty, noise and source confusion, we choose to adopt a single approach for *all* our sources, namely to use a fixed search radius. Next we have to choose a value for this radius, outside of which we reject sources. We are confident that our Super-map *as a whole* has astrometry reliable to within 3 arcsec, as pointing corrections were rarely much larger, and in addition because the stacked radio/submillimetre flux density begins to drop if the map is shifted by more than this (see Section 4.1). As some parts of the map are dominated by single observations, we need to consider the typical 2 arcsec pointing uncertainty of the James Clerk Maxwell Telescope (JCMT) as well.

The Monte Carlo simulations described in Paper I indicate an additional uncertainty of at most 5 arcsec for the simulated sources recovered at 850 μm, which is caused by a combination of confusion and residual sky noise altering the centroid of these faint sources. Adding these in quadrature leads to a conservative search radius of 7 arcsec, which is comparable to values chosen by other groups. Although this choice of search radius is somewhat arbitrary, we now show that it is in some sense an 'optimal' value.

3.1 An alternative to the *P*-statistic

Given the large positional uncertainty for SCUBA sources, several objects from an image in another waveband with higher resolution are possible counterparts to a given SCUBA source. However, which one is the correct identification? A measure often adopted by the submillimetre community is the so-called '*P*-statistic' (e.g. Downes et al. 1986). A different approach, and one we advocate and derive next, is to compare the *ensemble* of SCUBA positions to see which types of counterparts are most likely to be associated with the submillimetre detections.

Given a surface density of some class of object of n per unit area, the random probability that one or more lies within a distance θ of a specific SCUBA source is

$$P = 1 - \exp(-\pi n \theta^2). \quad (1)$$

This is the traditional *P*-statistic, and the lower its value, the less likely it is that the object is associated with a source by chance. Table 1 lists the radii within which there is a 95 per cent chance that the object is the counterpart to the SCUBA galaxy. It can be misleading, however. For example, if an ERO was found 9.3 arcsec away from a SCUBA source, the *P*-statistic would suggest there is only a 5 per cent chance it is not the correct counterpart. However, this object should have been rejected outright because it lies well outside the estimated 7 arcsec uncertainty in the SCUBA position.

Identifying counterparts between catalogues of objects at different wavelengths is an endeavour with a long history in the radio and X-ray communities (see, for example, de Ruiter, Arp & Willis 1977; Prestage & Peacock 1983; Stocke et al. 1991). The '*P*-statistic' is not the only approach used, and there are many discussions in the literature of how to use special properties of candidate counterparts, how to include astrometric uncertainties, cuts on flux ratios, etc. However, these discussions tend to be focused entirely on identifying each individual source.

As the detailed nature of SCUBA-bright galaxies is still largely unknown, then when comparing with other wavelength images, it is also useful to have a statistic which assesses the identification of the SCUBA sample as a whole. Such a statistic is also easier to interpret, particularly if we choose a fixed search radius. For what follows we assume a uniform probability of association over a 7-arcsec radius circle and zero outside. We can then straightforwardly estimate the probability of finding a set of objects within the search radius using Poisson statistics, as follows.

Given a population with a surface density of n, the probability of finding *no* sources within a distance, θ, of a given point is $p_0(\theta) = \exp(-\pi n \theta^2)$ (for a derivation see, for example, Scott & Tout 1989). This is just the same statement as in equation (1), and deals with the statistics of a single object. The probability that no counterparts are found for M independent searches (e.g. in our case for M separate SCUBA sources) is

$$p_{0,M}(\theta) = \Pi_1^M p_0(\theta) = p_0^M(\theta). \quad (2)$$

Similarly, the probability of finding a single counterpart is

$$p_{1,M}(\theta) = M p_0(\theta)^{M-1}[1 - p_0(\theta)]. \quad (3)$$

Table 1. Statistical measures for assessing the reliability of counterparts. For each of the catalogues we use in this paper, we tabulate several quantities. The first, θ_5 per cent is the separation out to which there is a 5 per cent probability that a source is not the correct counterpart. The second, p_0 should be read as 'the random probability that none of the M SCUBA sources have at least one counterpart within our adopted 7-arcsec search radius'. We then give the number K of M SCUBA sources that have an identifications within 7 arcsec. Note that some of the catalogues do not extend over the entire region of the Super-map. Finally, we give p_{K+}, the probability of K or more of the M SCUBA objects having at least one counterpart. We present these statistics both for our $>4\sigma$ SCUBA sources and for the full $>3.5\sigma$ catalogue. Here, LBG means 'Lyman break galaxy' and ERO is an 'extremely red object'.

Class	Number within survey area	θ_5 per cent arcsec	$>4\sigma$ sources			$>3.5\sigma$ sources		
			p_0	K/M	p_{K+}	p_0	K/M	p_{K+}
VLA 1.4 GHz	135	8.8	0.54	11/19	$p_{10+} < 10^{-10}$	0.33	14/34	$p_{14+} < 10^{-12}$
VLA 8.5 GHz	51	14.2	0.79	6/19	$p_{6+} < 10^{-7}$	0.66	7/34	$p_{7+} < 10^{-6}$
ISO 15 μm	99	4.1	0.26	4/9	$p_{4+} = 0.03$	0.14	6/13	$p_{6+} < 10^{-2}$
LBG	132	5.6	0.38	1/12	$p_{1+} = 0.62$	0.23	1/18	$p_{1+} = 0.77$
Chandra 2 Ms	328	5.4	0.20	8/19	$p_{8+} < 10^{-4}$	0.06	14/34	$p_{14+} < 10^{-6}$
$R_{\rm AB} < 24$	2626	2.0	0.00	9/19	$p_{9+} = 0.59$	0.00	17/34	$p_{17+} = 0.45$
$R_{\rm AB} < 22$	454	4.8	0.12	1/19	$p_{1+} = 0.88$	0.02	3/34	$p_{3+} = 0.70$
$R_{\rm AB} - HK'_{\rm AB} > 3.00$	801	3.7	0.03	4/19	$p_{4+} = 0.41$	0.00	7/34	$p_{7+} = 0.36$
$R_{\rm AB} - HK'_{\rm AB} > 3.93$ (ERO)	121	9.3	0.58	0/19	$p_{0+} = 1.00$	0.37	1/34	$p_{1+} = 0.63$

The pre-factor M is needed because there are M different ways to pick a single object from a set of M objects. Using a similar argument, the probability that of the M points, K have at least one counterpart is

$$p_{K,M}(\theta) = \frac{M!}{(M-K)!K!} p_0(\theta)^{M-K}[1 - p_0(\theta)]^K. \quad (4)$$

Therefore, of M objects, the probability that K or more of them have at least one counterpart is

$$p_{K+} = \sum_{i=K}^{M} p_i, \quad (5)$$

where we have dropped the M and θ. Note that $p_0 + p_{1+} \equiv 1$.

We have applied this statistic to our data and present the results in Table 1. Note how striking some of the implications are. For instance, the probability that 11 of the 19 SCUBA sources have a 1.4-GHz radio source within 7 arcsec just by chance is essentially zero.

Still, one has to treat this statistic with some degree of caution. For example, these probabilities assume that the populations are unclustered; as we will comment on later in this paper, clustering evidence does exist for some of the populations we compare the SCUBA sources against. We simply state this caveat for now, and will describe clustering results on a case-by-case basis later.

Finally, is the choice of a 7-arcsec search radius a good one? For larger radii, one will find more counterparts, but the probability of more matches by chance will also increase. Therefore, a trade-off exists between search radius and probability, and by calculating p_{K+} as a function of radius, we indeed find a minimum at 7 arcsec. This is independent of which catalogue is used to compute the statistic.

3.2 Statistical measures of submillimetre flux density from known objects

One can compare a catalogue of objects against a submillimetre image via a 'stacking' analysis in order to obtain a sense of the average submillimetre properties of the sample. The procedure is to take a list of detected objects from a survey, make cuts of some sort (if desired), and then sum up the flux density from a map at the positions of all the objects. Specifically, we take

$$\bar{S} = \frac{\sum_i S_i \sigma_i^{-2}}{\sum_i \sigma_i^{-2}}, \qquad (d\bar{S})^2 = \sum_i \sigma_i^{-2}, \quad (6)$$

where S_i and σ_i are the submillimetre flux density and error estimates at the position of object i. This technique is not restricted to submillimetre maps; for instance, Nandra et al. (2002) have compared a sample of Lyman break galaxies (LBGs) against *Chandra* X-ray maps.

It is important to check for systematic effects in these analyses. We take the list of 51 stars in the HDF-N region from the work of Mendez & Guzman (1998) and correlate them against the HDF Super-map. One would expect no signal from these stars as they are not submillimetre emitters. The stacked average, -0.20 ± 0.15 mJy, is consistent with both the average value of the map (0.02 mJy), and the distribution of fluxes derived from many realizations of taking 51 random positions in the map. Therefore, we can proceed with some assurance that any significant stacked signal is real.

Another effect to consider is the variation in the number of objects being compared. For large N, the stacked flux density will approach the average value of the map if the objects are distributed randomly on the sky. Therefore, the stacked flux density from N_1 objects cannot be directly compared with that from N_2 objects if they are significantly different (unless a correction is made). Hence in our stacking analyses we only make comparisons among subsamples with an equal number of objects.

4 MULTIWAVELENGTH DATA BASE AND SUBMILLIMETRE PRE-SELECTION CRITERIA

We have obtained source catalogues and images of the HDF-N over a wide range of wavelengths that are relevant to understanding the nature of the sources detected in the submillimetre maps. Before discussing the submillimetre objects individually, we present an overview of each catalogue and explain their relation to the submillimetre population. In particular, we will search for any criterion that make it possible to pre-select submillimetre detections in our map. We will start with the radio associations, which, as seen in Table 1, are certainly the most important link to the SCUBA population.

4.1 VLA and WSRT radio observations

The entire region of our Super-map has been imaged to roughly 9-μJy rms using both the Very Large Array (VLA) (Richards 2000) and the Westerbork Radio Telescope (WSRT) (Garrett et al. 2000) radio telescopes at 1.4 GHz. A smaller area survey, covering 11.3 × 11.3 arcmin^2 surrounding the central HDF region, was conducted with the VLA at 8.5 GHz (Richards et al. 1998) to an rms of 1.6 μ Jy. We have obtained the catalogues from each survey and the VLA maps at both frequencies in order to perform comparisons with our submillimetre map. Within the HDF-N Super-map there are 135 1.4 GHz VLA sources detected at $> 5\sigma$. In the combined 8.5-GHz catalogues (the primary list plus some fainter, less securely detected objects), there are 51 sources, 26 of which have a 1.4-GHz counterpart within 3 arcsec. We note that the WSRT and VLA 1.4-GHz catalogues generally agree, except that the WSRT positions are, on average, 1.5 arcsec west of the VLA positions. Unless otherwise noted, we will use the VLA catalogue.

Within the 7-arcsec search radius, 11 (six) of the 19 objects from the Super-map 4σ list have a 1.4- (8.5-) GHz radio counterpart. Seven of these radio sources are detected at both 1.4 and 8.5 GHz. As shown in Table 1, the chance of 11 SCUBA objects having a nearby radio source just at random is less than 10^{-10}. Based on this result we will assume that a radio source within 7 arcsec is the correct SCUBA counterpart, unless other compelling evidence excludes it.

4.1.1 Radio source stacking analysis

When we stack all the 1.4-GHz radio positions on the Super-map, we calculate an average 850-μm flux density of 1.8 ± 0.1 mJy. This is a very significant detection, and comparable to results from Barger, Cowie & Richards (2000) and Chapman et al. (2002a). To see if there are correlations between radio objects and the sources we *do not* detect, we mask out a circular region of radius 8 arcsec (the half-width of the beam size at 850 μm) from each of the detected submillimetre sources in the full $> 3.5\sigma$ catalogue. The 850-μm flux density stacked at the radio positions is still $S_{850} = 0.6 \pm 0.1$ mJy, suggesting that although the bulk of the radio-stacked flux density comes from the submillimetre-detected sources, additional flux density associated with radio galaxies which are weakly detected in the submillimetre range is still present. Stacking the 8.5-GHz sources yields an average 850-μm flux density of $S_{850} = 1.7 \pm 0.1$ mJy, and drops to 0.3 ± 0.2 when the SCUBA sources are masked out.

Radio galaxies are often characterized by the slope of their spectrum ($f_\nu \propto \nu^{-\alpha_r}$). Roughly speaking, an inverted spectrum ($\alpha_r < 0$) indicates the presence of self-absorbed synchrotron radiation from an active galactic nucleus (AGN). Flat spectra ($0 < \alpha_r < 0.5$) also suggest self-absorption and AGN, but in addition can be due to increased high-frequency radio emission from star formation. Steeper values of the index are associated with diffuse synchrotron radiation from star-forming galaxies (Condon 1992), with the 'canonical' index being 0.8. In Fig. 1 we plot the 850-μm flux density at the position of the 30 galaxies detected at both 1.4 and 8.5 GHz (see table 5 in Richards 2000) against the radio spectral index. The sample with $\alpha_r < 0.5$ is not significantly detected in the submillimetre band, but the 'star-forming' sources are.

4.1.2 Registering submillimetre images using radio data

Based on the strength of the submillimetre/radio correlation we can test the astrometry of the submillimetre map by shifting it and recalculating the stacked flux density at the radio positions. In Fig. 2 we plot the result. The correlation (as determined by the stacked flux) decreases quickly for distances greater than a SCUBA beam-size. A slight offset of 1.5 arcsec is seen between the VLA and SCUBA maps with a consistent shift found using only the positions of the

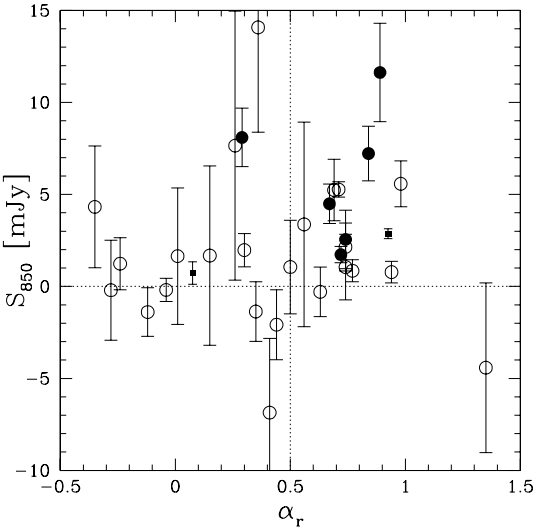

Figure 1. Comparing the SCUBA 850-μm flux density against the radio spectral index, α_r. Open circles are sources undetected with SCUBA, while solid ones represent radio galaxies found within 7 arcsec of a submillimetre source from the $> 4\sigma$ catalogue. Solid squares represent the stacked flux density in two bins of α_r (with each bin containing 15 sources).

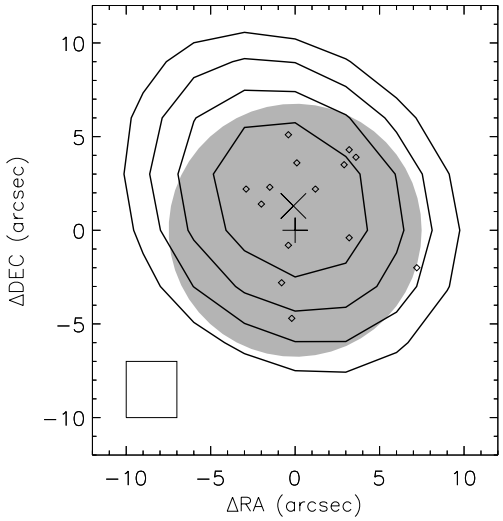

Figure 2. Using the VLA radio sources to test the submillimetre astrometry. We shift the radio map relative to the Super-map and calculate the stacked 850-μm flux density. Contours are drawn at 0.5, 0.6, 0.7 and 0.8 times the peak value of the stacked flux density. The grey circle is the same size as the SCUBA beam (FWHM), while the black square is the size of a pixel in the submillimetre Super-map (3 arcsec). Note that the contour at 0.5 is essentially the FWHM of the correlation distribution, and thus can be directly compared with the grey circle. The contours are more extended due to a combination of astrometry shifts in the Super-map and clustering. The contours prefer a centre (shown by the cross symbol) that is offset by roughly 1.5 arcsec (half a pixel) from the unshifted submillimetre map (denoted by the plus symbol). Diamonds denote the offsets for the 14 radio sources which we later claim are the correct identifications to submillimetre sources in the HDF-N.

radio counterparts to our SCUBA sources. Although no result in this paper is sensitive to such a small offset, we make the shift in order to have the best astrometry for the SCUBA Super-map. Consequently, some of the 'SMMJ' source names have changed by one digit from the list in Paper I. Note that the correlation in Fig. 2 seems to extend past the size of a theoretical, diffraction limited SCUBA beam. This would be the case if individual scans had small offsets between them and were then co-added. Fitting the FWHM of the brightest sources in the Super-map does show that some objects have profiles up to 15 per cent wider than the nominal 15-arcsec beam. However, it is also possible that there is a contribution from clustering of the radio sources. As noted in Richards (2000), there is a $> 5\sigma$ detection of radio source clustering on scales of $\sim$0.1–2.0 arcmin.

4.2 *Chandra* X-ray imaging

ACIS, the Advanced CCD Imaging Spectrometer (Nousek et al. 1987) on board *Chandra* performed a 2-Ms integration on a 17×17 arcmin^2 region surrounding the HDF-N, making it the deepest X-ray observation yet obtained. The survey reaches 0.5–2.0 keV (soft) and 2–8 keV (hard) flux limits of about 3×10^{-20} and 2×10^{-19} W m^{-2}, respectively (Alexander et al. 2003b). To examine the relationship between SCUBA sources and X-ray flux, we use the *Chandra* HDF-N catalogue of Alexander et al. (2003b) that covers our entire submillimetre map. The catalogue lists 503 objects, 451 in the soft band and 332 in the hard band, with many sources detected in both. The positions are accurate to within 0.3 arcsec near the centre of the field, but the uncertainty increases to 1.5 arcsec near the edge. Of these detections, 328 fall within our submillimetre map, and eight of the 19 SCUBA sources have an X-ray source within our 7-arcsec search radius (three of these have two X-ray sources within 7 arcsec).

4.2.1 *Chandra stacking analysis*

We can characterize the spectral shape of the X-ray emission via the hardness ratio, $(H - S)/(H + S)$. For this purpose it is conventional to use the counts in the hard (H) and soft (S) bands instead of the fluxes. Fig. 3 reveals a strong correlation between those sources with a hard X-ray spectrum and stacked submillimetre flux density. We obtain an overall average 850-μm flux density of $S_{850} = 1.0 \pm 0.1$ mJy. Most of this signal comes from the hardest third of the sources, although even the softer ones are significantly detected. In general, the stacked flux density is due to SCUBA-detected objects, and not from X-ray-detected objects that are faint in the submillimetre range. This is in stark contrast with the radio stacking results.

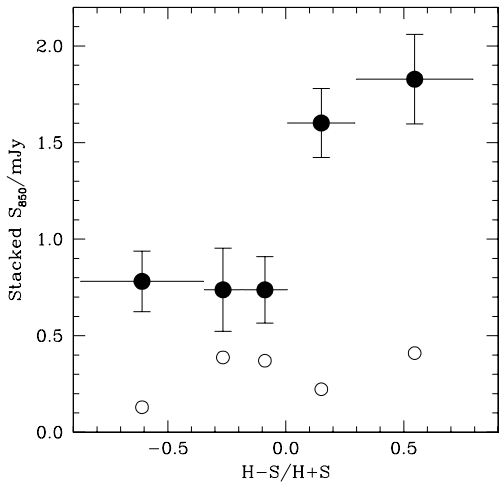

Figure 3. The stacked submillimetre flux density as a function of the X-ray hardness ratio. We have split the *Chandra* sources into five equal-sized bins, with roughly 65 objects per bin. Solid circles show binned averages, with horizontal bars denoting the size of the bins. The open circles (with error bars omitted for clarity) are the same but with the detected SCUBA sources masked out.

Within our 7-arcsec search radius we find eight *Chandra* sources out of $19 > 4\sigma$ SCUBA sources, and 14 in the full $> 3.5\sigma$ catalogue. However, with over twice as many X-ray-detected objects (in the *Chandra* catalogue) than radio objects, the probability of a chance occurrence is much higher. None the less, the probability of this many matches is $<10^{-4}$ (as shown in Table 1), and therefore highly significant. This estimate could be biased if the SCUBA sources cluster around X-ray galaxies, as we now discuss.

4.2.2 *The clustering of submillimetre and X-ray sources*

Almaini et al. (2002, 2003) claim to detect a strong clustering signal between SCUBA and X-ray sources in the UK 8-mJy survey (Scott et al. 2002). They determined that although only one of 17 SCUBA sources in the 8-mJy catalogue had a genuine *Chandra*-detected counterpart, X-ray and SCUBA sources tend to be found close together. The clustering signal at small angular separations can be due to objects which are the same galaxy identified at both wavelengths. However, a positive correlation out to $\sim$1 arcmin must be due to the two populations tracing out the same large-scale structure. Hence the 8-mJy results imply a spatial link between X-ray bright and submillimetre bright populations. It has been speculated that these two catalogues trace the same population, but at different stages in their evolution. This would explain why there is no enhanced overlap between SCUBA and X-ray sources, yet a clustering signal between the two populations can still be detected. High-redshift clusters cover angles $\sim$1 arcmin, which is consistent with this picture.

We performed a clustering analysis for sources found within the HDF-N Super-map using the statistic (Hamilton 1993)

$$w(\theta) = \frac{SX\ R_{\rm X}R_{\rm S}}{SR_{\rm X}\ XR_{\rm S}} - 1, \qquad (7)$$

where $w(\theta)$ is the angular correlation function and the pairs of sources are counted between different catalogues: S and X represent SCUBA and X-ray sources, while $R_{\rm X}$ and $R_{\rm S}$ are random X-ray and SCUBA catalogues. Monte Carlo simulations are required to generate the random catalogues. In these simulations, we assume that the sensitivity to X-ray sources is the same across the entire field, and can therefore place sources randomly on the sky using simple Poisson statistics. This is not precisely true, as the X-ray sensitivity decreases with off-axis distance. However, the sources we are using are quite significantly detected and therefore we can safely assume that we are not biasing our results. We cannot make the same assumption for the SCUBA-detected galaxies, as the sensitivity is far from uniform across the field. Therefore, we generated 500 simulated maps using the submillimetre source count model described in Paper I. Using these random catalogues and the estimator in equation (7), we calculated $w(\theta)$ for 30-arcsec wide angular bins, and plot the results in Fig. 4. No clustering signal is found.

Why is there a discrepancy between the 8-mJy results and those here? First we note that of the seven SCUBA sources with an X-ray source nearby, only three are brighter than the sensitivity limit of the X-ray observations in the 8-mJy region. Thus we repeated the analysis ignoring X-ray sources fainter than the 8-mJy sensitivity, but

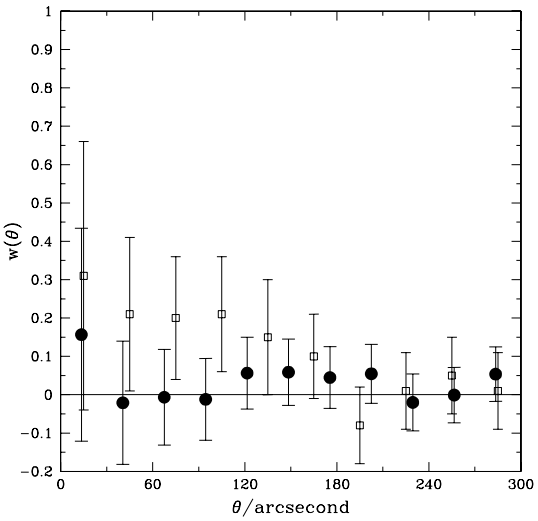

Figure 4. Clustering between SCUBA and X-ray-detected objects. Solid circles show the cross-clustering estimate based on our $> 4\sigma$ sources and the published X-ray coordinates from *Chandra*. No detection is seen. Open squares are from Almaini et al. (2002), which show some weak evidence of clustering, though using only the *Chandra* 1-Ms data and the shallower HDF-N SCUBA map in Borys et al. (2002). We have ignored X-ray sources closer than 7 arcsec, as those are generally the SCUBA sources themselves.

still no correlation was found. One idea is that the measured clustering signal is due to gravitational lensing of SCUBA sources behind the foreground large-scale structures that host the X-ray objects (Almaini et al. 2003). If this were true, one might expect a stronger signal when using only the brightest (and presumably more strongly lensed) SCUBA sources, as the steepness of the source-counts here leads to a stronger bias in the number of objects detected. We therefore re-did the clustering analysis using only the > 7 mJy sources but still found no detection. Even including the $> 3.5\sigma$ detections to increase the sample size did not help.

We conclude there is no evidence of an X-ray/SCUBA clustering correlation in the HDF, and speculate that this may be due to field-to-field variation. On the other hand, Almaini et al. (2002) only report weak clustering in their HDF-N analysis. We also note that Almaini et al. (2003) used a different $w(\theta)$ estimator than that given in equation (7). This estimator is not symmetric between the submillimetre and X-ray ranges, and thus may be prone to bias.

In defence of the foreground lensing hypothesis, there is one SCUBA object, SMMJ123621+621252, which has seven *Chandra* detections within 20 arcsec none of which are the counterpart to the SCUBA source. This object is discussed in the next section. There are also two SCUBA sources in a crowded field (based on optical images) that have an apparent *Chandra* identification with a spectroscopic redshift, though the redshift is too low to be consistent with the radio–FIR (far-infrared) correlation. These examples may indicate systems where foreground sources lens the background SCUBA galaxy. However, these are anecdotal suggestions, and we stress that we could find no statistical evidence for such associations.

4.2.3 Are Chandra sources a good way to identify SCUBA-bright galaxies?

Of the eight SCUBA galaxies that have a *Chandra*-detected galaxy within 7 arcsec, only two were not first detected in the 1.4-GHz radio map: SMMJ123637+621155 and SMMJ123656+621201. In both cases, there is a radio detection that we call the counterpart, but the X-ray point source is not coincident with it. A third object, near SMMJ123652+621225 does have a radio identification, but (as explained in the next section) is not the correct counterpart.

Thus we conclude that all secure SCUBA identifications that have a *Chandra* detection are also seen in the 1.4-GHz radio maps. Indeed, the radio band is much more efficient, with a success rate here of 10/18 compared with 5/18 objects (ignoring the peculiar object SMMJ123652+621225). The count rates for these five *Chandra* sources are such that only one would have been detected by *Chandra* in an exposure time equivalent to that used for the VLA 1.4-GHz image ($\sim$50 h). So, per unit integration time, it is currently much more efficient to find SCUBA counterparts with the VLA than with *Chandra*.

4.2.4 X-ray properties of SCUBA objects

Including sources from the supplementary SCUBA catalogue, we present a list of 10 X-ray-detected SCUBA objects in Table 2; five from the $> 4\sigma$ list and five from the supplemental catalogue. Only four are in common with the list of seven presented in Alexander et al. (2003b). From that work, which used the previous

Table 2. X-ray properties of SCUBA sources with secure identifications. All X-ray quantities are obtained from the *Chandra* 2-Ms catalogue (Alexander et al. 2003b). Fluxes are in units of 10^{-18} W m^{-2}. 'FB', 'SB' and 'HB' refer to the full, soft and hard bands, respectively. Redshifts are taken from Table 5, and luminosities are calculated using the prescription in Alexander et al. (2003a).

SMM ID	X-ray counts	Hardness ratio	Effective Γ	X-ray flux FB	SB	HB	$S_{1.4}$ (μJy)	z	$\log(L_X)$ (erg s^{-1})	$\log(L_{1.4})$ (W Hz^{-1})
850-μm detections $> 4\sigma$										
J123616+621516	130.4	-0.09	$1.0^{+0.2}_{-0.2}$	1.02	0.18	0.80	53.9 ± 8.4	2.06	24.1	43.5
J123645+621449	12.6	< 0.00	1.4	0.08	0.03	0.14	124.0 ± 9.8	$1.9^{+1.0}_{-0.7}$	24.4 ± 0.4	42.3 ± 0.5
J123650+621316	27.2	-0.39	1.4	1.64	0.61	<1.23	49.2 ± 7.9	0.475	22.6	42.1
J123701+621146	14.1	< -0.18	1.4	0.09	0.04	< 0.12	128.0 ± 9.9	1.52	24.2	42.1
J123707+621410	84.4	$+0.24$	$0.4^{+0.2}_{-0.2}$	0.98	0.09	0.91	45.3 ± 7.9	$3.7^{+2.8}_{-1.5}$	24.6 ± 0.4	44.1 ± 0.6
Additional 850-μm detections $> 3.5\sigma$										
J123607+621019	59.1	$> +0.36$	$0.1^{+0.1}_{-0.1}$	0.74	< 0.05	0.77	74.4 ± 9.0	0.47	22.8	41.8
J123608+621431	37.6	< -0.22	1.4	0.25	0.08	< 0.22	68.9 ± 8.8	0.472	22.7	41.3
J123628+621046	198.4	$+0.34$	$0.2^{+0.2}_{-0.2}$	2.31	0.17	2.23	81.4 ± 8.7	1.013	23.6	43.1
J123635+621237	53.3	< -0.42	$1.6^{+1.6}_{-1.6}$	0.29	0.10	< 0.17	230 ± 14	1.219	24.2	42.4
J123652+621352	20.4	< -0.03	1.4	0.13	0.03	< 0.14	< 45	1.355	< 23.6	42.2

releases of HDF-N submillimetre data, we have rejected SMMJ123622+621618 because its large distance from the submillimetre galaxy renders it an unlikely identification. SMMJ123618+621552 is in a region of extended X-ray flux, and we were unable to determine if a point source was present. Alexander et al. (2003b) re-reduce the data using different detection parameters and do find a source here, but we choose to employ only the original 2-Ms catalogue. Neither of the two *Chandra* galaxies in the vicinity of SMMJ123713+621204 stand out as the correct identification, so we reject those as well.

For these *Chandra* identifications we calculated radio and X-ray luminosities using the formulae given in Alexander et al. (2003a). We assumed a radio spectral index of 0.8 and an unobscured photon index of $\Gamma = 2$ for each source. These results are summarized in Table 2 and Fig. 5.

The luminosities of most of the sources lie within the range determined by Bauer et al. (2002) and Shapley, Fabbiano & Eskridge (2001) for local star-forming galaxies. Four sources lie above the relation, however, suggesting an AGN component. Alexander et al. (2003a) use templates of various galaxies and quasars to argue that, although these systems harbour an AGN, their FIR luminosity is still dominated by star formation (see also Farrah et al. 2003). Better constraints on the FIR luminosity (via observations at other submillimetre wavelengths) along with optical spectroscopy could be used to strengthen this argument, but such data are not yet available for a significant sample.

4.3 Optical–near-infrared imaging

The most comprehensive published optical survey, aside from the *Hubble Space Telescope* (*HST*) imaging itself, is presented in Capak et al. (2004). They obtained deep optical and near-IR (NIR) images covering the entire HDF-N Super-map in the U, B, V, R, I, z' and HK' bands, and made the images and catalogues publicly accessible via their web page. We use their R and z' selected catalogues (consisting of almost 49 000 objects) which cover a 0.2 deg^2 region. The submillimetre map is completely contained within this area.

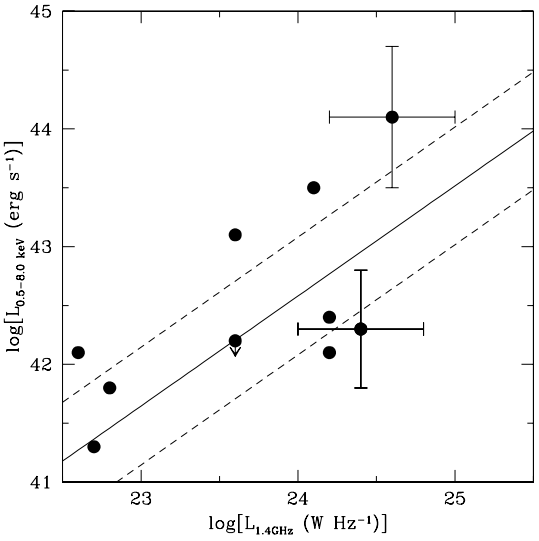

Figure 5. Radio/X-ray luminosity relation for secure SCUBA detections. The solid and dashed lines represent the best fit (and $\pm 1\sigma$ range) of the relation as derived by Bauer et al. (2002) for a sample of local galaxies (Shapley et al. 2001).

The catalogue uses the AB magnitude system, and we conform to that convention here unless otherwise noted.

With so many sources, it is impossible to distinguish which are the correct counterparts to the SCUBA detections without some other information, so we now examine the submillimetre properties of various subsamples of optical–NIR-detected galaxies.

4.3.1 *Optically Faint Radio Sources (OFRS)*

Observations by Barger et al. (2000) and Chapman et al. (2001a) find that optically faint (I(Vega) > 25) galaxies detected using deep 1.4-GHz radio observations are coincident with $\simeq 70$ per cent of SCUBA sources with fluxes above 5 mJy. This population has been extensively modelled (Chapman et al. 2002a, 2003a) and exploited to obtain spectroscopic redshifts of the optically detected host galaxies (Chapman et al. 2003b).

We searched for I(Vega) > 24 galaxies within 2 arcsec of a 1.4-GHz radio detection, and found 17 candidates. There were an additional 13 radio sources with no optical counterpart, for a total of 30 optically faint radio sources. Of these, nine are within 7 arcsec of a SCUBA-detected object. These form a subset of the 11 1.4-GHz detections found coincident with SCUBA objects without any other selection criteria. Therefore, the optically faint radio sources (OFRS) have a $9/30 = 30$ per cent success rate in picking out SCUBA sources in the HDF-N, while the radio sources alone give only $10/135 = 7$ per cent. Thus OFRS are more effective at selecting submillimetre bright galaxies than radio alone. We do not find as high a rate as some other studies, but it is unclear that these fractions can be applied directly to other surveys; in the HDF-N Super-map the sensitivity to submillimetre sources is strongly variable across the field. If we restrict this analysis to the region of the submillimetre map that has an rms noise of 1.5 mJy or lower, there are six out of 13 optically faint radio sources coincident with SCUBA detections (46 per cent).

4.3.2 *Galaxies with red optical–NIR colours*

The dust responsible for the extreme IR luminosities that SCUBA detects is also responsible for reddening the optical–ultraviolet (UV) spectrum, making such galaxies appear very red compared with the field population. Wehner, Barger & Kneib (2002) compared 850-μm flux densities against a list of galaxies detected with K'(Vega) < 21.25, finding a significant trend of increasing submillimetre flux density with increasing optical–NIR redness. Fig. 6 presents the results from a similar analysis we conducted using the HDF-N maps. In general, the fainter, redder galaxies are more submillimetre bright. However, we cannot easily separate the effects of redness from faintness, as they are correlated (see the left-hand part of the middle panel of Fig. 6). There is weak evidence that the stacked flux density does not continue to rise for the most extremely red sources, though the completeness at these faint flux levels is lower. One important thing to note is that the stacked average is dominated by *detected* sources, a point also raised in Webb et al. (2004).

The criterion $R - K > 5.3$ (Vega) can be used to define an ERO, motivated by being the approximate colour of an elliptical galaxy at $z = 1$. Applying a correction to the HK' magnitudes to convert to K (P. Capak, private communication), we calculate that $R - HK' > 3.9$ is the equivalent criterion in AB magnitudes. We find 121 EROs within the Super-map. However, the stacked flux density at their positions is only 0.22 ± 0.16 mJy, indicating that EROs themselves are a poor way to pre-select SCUBA galaxies. This result echoes

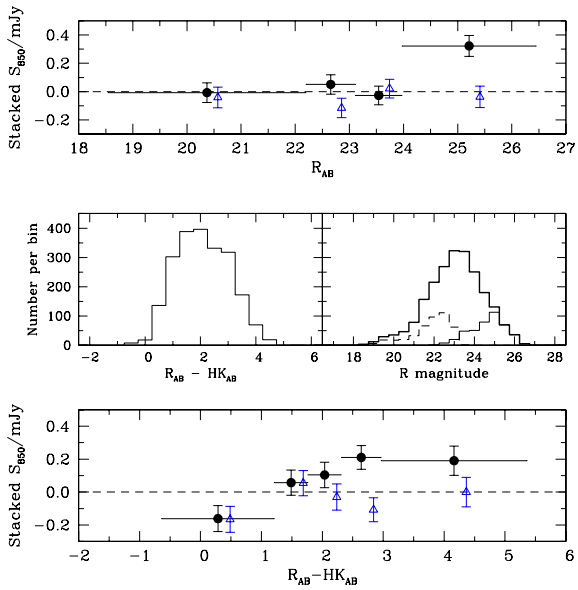

Figure 6. The top panel shows the stacked 850-μm flux density as a function of *R*-band magnitude, showing a marked increase toward optically fainter objects. Filled circles denote the average submillimetre flux density in each bin, the width of which is given by the horizontal bars, chosen to ensure that there are the same number of objects in each bin. Triangles correspond to the same bins (offset for clarity), but first removing the known submillimetre sources from the entire $> 3.5\sigma$ SCUBA catalogue. The central left-hand panel simply shows the distribution of $R - HK'$ values from the catalogue of Capak et al. (2004). On the right, we plot the distribution of *R*-band magnitudes (thick line) as well as the subset of *R*-band fluxes from the reddest (thin line) and bluest (dashed) bins. This shows a trend for the redder sources to be fainter, which means we cannot completely separate colour effects from brightness effects. The bottom panel plots the stacked 850-μm flux density for five bins selected by colour. The redder objects are statistically detected, but with no detection once the $> 3.5\sigma$ SCUBA sources are removed (triangles).

that of Mohan et al. (2002), who targeted a sample of 27 EROs with SCUBA and detected none down to an rms of ∼2 mJy. Only a single SCUBA source in our catalogue has an ERO within 7 arcsec (SMMJ123700+620910), and that was already detected in the radio band. However, one has to be careful with direct comparisons, as the near-IR data we have used are shallower than those available in some other fields, and it may well be that one finds a higher ERO rate with deeper *K*-band imaging.

4.3.3 Optical LBG drop-out surveys

Because of their inferred high star formation rates and large co-moving number density, Lyman-break galaxies (Steidel et al. 1998) make an interesting target for submillimetre studies. Using reasonable conversion factors based on local standards, the predicted 850-μm flux densities are expected to be of the order of 5 mJy. However, submillimetre surveys to date have failed to detect LBGs, except in a handful of cases (Chapman et al. 2000, 2001b; Peacock et al. 2000; Webb et al. 2003a).

The HDF-N Super-map covers much more area than previous attempts, and contains many more known LBGs. Steidel et al. (2003) find 132 LBG candidates (selected photometrically) in a 73 arcmin^2 region within the HDF. However, the stacked 850-μm flux density is 0.03 ± 0.10 mJy confirming previous results that LBGs are typically

Table 3. Optical galaxies within 7 arcsec of radio-detected SCUBA galaxies in the HDF-N. Here θ is given in arcsec, and magnitudes are in the AB system. A 'Y' in the last column indicates that the galaxy is radio-detected.

Object Name	K	$(R-K)$	θ	Radio
SMMJ123616+621516	22.4 ± 0.3	1.5 ± 0.3	3.1	
	23.3 ± 0.6	2.1 ± 0.6	4.2	Y
SMMJ123618+621552	22.8 ± 0.4	2.4 ± 0.4	3.5	Y
	>22.1	<3.0	6.6	
SMMJ123645+621449	>22.1	<3.5	1.9	
	>22.1	<4.1	2.2	Y
	23.2 ± 0.4	2.1 ± 0.4	2.9	
	22.8 ± 0.3	1.1 ± 0.3	3.2	
	22.8 ± 0.3	2.2 ± 0.3	5.4	
SMMJ123650+121316	21.4 ± 0.2	2.4 ± 0.2	0.6	
	19.9 ± 0.1	0.5 ± 0.1	5.5	
	20.4 ± 0.1	1.7 ± 0.2	6.7	Y
SMMJ123707+621410	22.4 ± 0.3	3.2 ± 0.3	4.3	Y
	22.3 ± 0.3	1.6 ± 0.3	4.6	
	>22.1	<3.9	6.7	
SMMJ123701+621146	21.4 ± 0.1	3.0 ± 0.1	2.6	Y
	>22.1	<4.2	3.8	
	22.2 ± 0.1	2.0 ± 0.1	4.9	
	22.0 ± 0.1	0.6 ± 0.1	4.9	
	23.0 ± 0.2	1.5 ± 0.2	5.9	

SCUBA-faint. We also performed a cross-clustering analysis like that described in the X-ray section, but failed to detect any signal.

In the HDF-N region, only two LBGs seem co-incident with a SCUBA source. SMMJ123656+621201 (also known as HDF 850.2) has a pair of possible LBG counterparts located within 5 arcsec. However, as we discuss in Section 5, this pair may not constitute the correct identification. In any case, submillimetre bright galaxies are much rarer than LBGs, with only one SCUBA galaxy (with $S_{850} > 5$ mJy) per 7 arcmin^2, compared with roughly eight LBGs (at $z \sim 3$) over the same area. Hence, even if there is complete overlap between the populations, number counts alone suggest that the typical LBG must have an average 850-μm flux density of a fraction of a mJy.

4.3.4 Are optical surveys a good way to identify SCUBA sources?

Webb et al. (2003b) argue that NIR-selected sources found in deep ($K_{AB} \sim 23$) imaging are just as effective at identifying SCUBA sources as 1.4-GHz images (with a 1σ rms of ∼16 μJy) in the CUDSS 14-h submillimetre field (Eales et al. 1999). However, this only relates to finding a counterpart of a *known* SCUBA source. We have explored various brightness and colour cuts and find that no optical-only criteria is successful at *pre-selecting* SCUBA galaxies.

Nevertheless, we can examine the optical properties of the radio sources to see if they have anything in common that can be used to select the counterpart to a known SCUBA detection. In Table 3 we present a list of the radio-detected SCUBA sources (from the $> 4\sigma$ catalogue) in the HDF-N with optical/NIR sources detected nearby. We restrict the list to the six radio-detected objects that have an optically detected counterpart. There is one additional source that meets this criterion (SMMJ123652+621225), but we exclude it from the list for reasons explained later.

We find that of the six SCUBA galaxies we are considering, three have the radio source also coincident with the optical source closest to the centroid. Still, one would be hard-pressed, without the radio

data, to decide between the objects around SMMJ123645+621449. In short, though some of the optical-only identifications would have selected the correct counterpart, there are many cases, especially in crowded fields, where it becomes too difficult to ascertain this with any confidence. We do note, however, that in half the cases we would have chosen the correct identification just by picking the reddest galaxy within 7 arcsec.

Webb et al. (2003b) also claim that clumps of two or more nearby EROs demarcate regions where a submillimetre source can be found. It is certainly interesting to see if regions of overdensity in one catalogue are good tracers of objects in another. Thus, we took the optical catalogues and counted the number of objects that have at least one neighbour within 10, 20, and 30 arcsec of another. We then assess how many submillimetre sources would be detected within the size of the SCUBA array if clumps of red galaxies were targeted.

For galaxies with colours $R - HK' > 3.9$ (EROs), we find six that have at least one neighbour within 10 arcsec. The three SCUBA pointings required to cover these six objects would have found a single source in our 4σ submillimetre catalogue. This is roughly the same efficiency as simply pointing the telescope at random spots on the sky. Overall, we can find no cut on the optical catalogues using spatial correlations, $R - HK'$ colour or magnitude that would allow us to pre-select regions where SCUBA sources would be found.

4.4 *ISO* mid-IR imaging

ISO observed a roughly $\sim 4 \times 5$ arcmin^2 area around the HDF-N at both 7 and 15 μm. The data were reduced separately by three different groups (Goldschmidt et al. 1997; Aussel et al. 1999; Désert et al. 1999), and here we use the 15-μm catalogue found in Aussel et al. (1999). They present a list of 49 objects with high SNR, and an additional 50 with lower confidence, covering a total area of 24 arcmin^2. The positions are accurate to within 3 arcsec.

Concentrating first on the 49 secure *ISO* 15-μm detections, we find a stacked 850-μm flux density of 0.65 ± 0.09 mJy, which drops to 0.16 ± 0.09 mJy after removing sections around SCUBA sources. The list of 50 less secure detections gives similar results, and the overall (99 sources) stacked flux density is significantly detected at 0.41 ± 0.06 mJy. The brightest third of the *ISO* sources ($S(15\ \mu\text{m}) > 150$ μJy) have the strongest stacked flux density, with an average value of 0.86 ± 0.13 mJy. We later conclude that only one object from our catalogue has a 15-μm counterpart, despite the low probability that four of 13 SCUBA galaxies would have an *ISO* source within 7 arcsec by chance (see Table 1). Of the other SCUBA sources with nearby *ISO* sources, one is identified with an unrelated radio source and the remainder are inconclusive.

5 COUNTERPARTS OF EACH SCUBA OBJECT

5.1 General criteria for counterpart identification

We now come to a detailed description of the counterparts of the SCUBA-detected objects. Of all the correlations presented thus far, the 1.4 GHz–850 μm overlap is by far the strongest. Thus in this section there will naturally be an emphasis on the radio sources. Based on the strength of this correlation, we will not only consider the sources formally detected at 5σ in the 1.4-GHz map presented by Richards (2000), but fainter ones as well. Richards (2000) find that the 1.4-GHz differential number counts are well fitted by a power law of index $\gamma = -2.4 \pm 0.1$. Assuming uniform noise, the number of sources brighter than an $n\sigma$ noise limit goes as $N(> 5\sigma)(n/5)^{1+\gamma}$. Thus for a 3σ cut, there are about twice as many sources. This is still small enough that chance overlap with a large number of SCUBA-detected galaxies is negligible. There is no question that a few of these fainter sources will be spurious, however, so we lend them weight only if there is an object detected in the optical, NIR or X-ray bands at the same position.

We will not assign a secure identification to SCUBA sources unless they are detected at $> 3\sigma$ in the radio band, but will offer tentative identifications for sources that are faint and red, or are the only object detected within the error circle. Together, this leads to a reasonable recipe for identifying counterparts for the SCUBA objects.

(i) Strongly detected ($> 5\sigma$) 1.4-GHz sources within 7 arcsec of the SCUBA centroid will be deemed to be the host of the submillimetre emission. Optical, NIR and X-ray properties will be based on the object that is coincident with the radio position (if any).

(ii) Weakly detected (3–5σ) 1.4-GHz sources within 7 arcsec, with a counterpart in another band that has similar or better resolution, will be chosen as the identification with the submillimetre source.

(iii) A detection in any band, within the search radius, will be flagged as a possible identification if and only if no other candidate in the vicinity is detected.

A description of each source, and images of each are presented in the appendices (Figs A1–A3). We summarize the counterparts in Table 4. We suggest 10 secure identifications in the $> 4\sigma$ SCUBA source list, and a further two tentative identifications, as well as five secure identifications for the 3.5–4.0σ sources and one tentative identification for the 450-μm sources. Although in each case the radio galaxy is used for the secure counterpart, our selection criterion apparently fails for the one special source we have alluded to throughout this paper.

5.2 The curious case of SMMJ123652+621225

The radio-detected *Chandra* galaxy 5.7 arcsec to the south-west of this SCUBA source is seemingly an obvious choice. However, deeper observations have revealed that this is not the case. This submillimetre source, usually called HDF 850.1, has been the subject of intense scrutiny since its discovery in the initial deep submillimetre survey of the HDF by Hughes et al. (1998). After years of effort, Dunlop et al. (2004) now claim that the counterpart for 850.1 has been determined.

Using the IRAM interferometer, the submillimetre flux was resolved with a positional uncertainty of ∼0.3 arcsec (Downes et al. 1999). However, it was not found to be coincident with the VLA source mentioned above, but rather a new and very faint radio source found by co-adding VLA and MERLIN data.

It cannot be stressed how difficult obtaining this (tentative) counterpart has been. Fortunately, the majority of SCUBA objects do not appear to suffer from being in a such a complicated system. Nevertheless, experience with this object only highlights the need for better angular resolution and sensitivity for submillimetre observations, as it calls into question the validity of *any* counterpart.

5.3 Available redshift information for the SCUBA sources in the HDF-N

Determining redshifts of the SCUBA population is critical in order to place these systems in their correct cosmological context, but this has proven difficult observationally.

Table 4. Multiwavelength summary of SCUBA detections. We give the source name, counterpart position and distance from the SCUBA centroid, radio, submillimetre, mid-IR, and optical/near-IR fluxes (or 3σ upper limits). Optical magnitudes are in the AB system. The X-ray fluxes are presented separately in Table 2. The symbols in the 'Bands' column are as follows: R means detected in the 1.4-GHz radio map; 8 is the 8.5-GHz radio; X is X-ray; I is Mid-IR (*ISO*); and O means an optical counterpart. The 'Comments' column indicates whether we regard the identification as secure or tentative. Gaps in the table mean that imaging was not performed at that position. For consistency, we provide the data on the radio source near HDF850.1, although this may not be the correct identification.

SMM ID	J2000 12h+	J2000 62°+	θ (arcsec)	$S_{1.4\,\mathrm{GHz}}$ (μJy)	$S_{8.5\,\mathrm{GHz}}$ (μJy)	$S_{850\,\mu\mathrm{m}}$ (mJy)	$S_{450\,\mu\mathrm{m}}$ (mJy)	$S_{15\,\mu\mathrm{m}}$ (μJy)	Optical R, $R-HK'$	Bands	Comments
					850-μm detections $> 4\sigma$						
J123607+621143				<45	<9	15.2 ± 3.8	<97				
J123608+621249	36:08.530	12:49.61	0.4	<45	<9	16.0 ± 3.7	<95		25.2 ± 0.1, <3.1	O	Tentative
J123616+621516	36:16.148	15:13.67	4.4	53.9 ± 8.4	<9	6.3 ± 0.9	<35		25.4 ± 0.1, 2.1	RXO	Secure
J123618+621007				<45	<9	6.6 ± 1.5	<66				
J123618+621552	36:18.328	15:50.48	3.5	151 ± 11	<9	7.2 ± 0.9	<34		25.2 ± 0.1, 2.4	RO	Secure
J123621+621252				<45	<9	12.1 ± 2.6	<85				
J123621+621710	36:21.272	17:08.40	2.5	148 ± 11	<9	8.8 ± 1.5	<72			R	Secure
J123622+621616	36:22.625	16:21.28	4.4	<45	<9	8.6 ± 1.0	51 ± 17		24.4 ± 0.1, <2.3	O	Tentative (pair)
J123634+621407				<45	<9	11.2 ± 1.6	<67	<200			
J123637+621155	36:37.565	11:56.32	4.0	40 ± 9	<9	7.0 ± 0.8	<46	<200		R	Secure
J123645+621449	36:46.049	14:48.69	2.2	124.0 ± 9.8	24.7 ± 4.5	8.5 ± 1.3	<47	<200	26.2 ± 0.2, <4.1	R8XO	Secure
J123650+621316	36:49.708	13:12.78	7.0	49.2 ± 7.9	<9	2.0 ± 0.4	<11	<200	22.1 ± 0.1, 1.7	RXOI	Secure
J123652+621225	36:51.760	12:21.30	5.7	49.3 ± 7.9	16.8 ± 2.3	5.9 ± 0.3	<12	<200	22.0 ± 0.1, 1.6		(HDF 850.1)
J123656+621201	36:56.605	12:07.62	5.8	46.2 ± 7.9	<9	3.7 ± 0.4	<16	<200		R	Secure
J123700+620910	37:00.256	09:09.75	1.5	324 ± 18	66.7 ± 13.7	8.6 ± 2.1	<85			R8	Secure
J123701+621146	37:01.574	11:46.62	2.3	128.0 ± 9.9	29.5 ± 2.8	4.0 ± 0.8	<27	<200	25.3 ± 0.1, 3.9	R8XO	Secure (ERO)
J123702+621301				<45	<9	3.4 ± 0.6	<25	<200			
J123707+621410	37:07.208	14:08.08	4.4	45.3 ± 7.9	29.0 ± 6.1	9.9 ± 2.5	<85		25.6 ± 0.1, 3.3	R8XO	Secure
J123713+621204				<45	<9	6.1 ± 1.4	<40				
					850-μm detections 3.5–4.0σ						
J123607+621019	36:06.850	10:21.38	3.2	74.4 ± 9.0	<9	13.5 ± 3.7	<97		24.4 ± 0.1, 2.8	RXO	Secure
J123608+621431	36:08.592	14:35.77	4.1	68.9 ± 8.8	<9	6.1 ± 1.7	<60			RX	Secure
J123611+621213				<45	<9	12.8 ± 3.4	<90				
J123628+621046	36:29.134	10:45.79	3.4	81.4 ± 8.7	<9	4.4 ± 1.2	<55		24.0 ± 0.1, 3.6	RXO	Secure
J123635+621237	36:34.515	12:41.01	7.6	230.0 ± 14	52.6 ± 4.7	3.0 ± 0.8	<41	363^{+79}_{-38}	23.4 ± 0.1, 2.6	R8XOI	Secure
J123636+620658				<45	<9	22.1 ± 5.6	<155				
J123647+621840				<45		19.5 ± 5.4	<154				
J123652+621352	36:52.76	13:54.1	2.0	<45	7.8 ± 2.8	1.8 ± 0.4	<16	<200	22.3 ± 0.1, 0.9	8XO	Secure
J123653+621119				<45	<9	2.8 ± 0.8	<40	<200			
J123659+621452				<45	<9	5.2 ± 1.4	<72	<200			
J123706+621849				<45		21.6 ± 5.8	<178				
J123719+621107				<45	<9	7.2 ± 2.0	<55				
J123730+621055				<45	<9	13.3 ± 3.6	<98				
J123730+621855				<45	<9	27.1 ± 7.6	<286				
J123741+621225				<45		23.7 ± 6.1	<185				
					450-μm detections $> 4\sigma$						
J123619+621127	36:19.370	11:25.6	2.0	<45	<9	<5.8	110 ± 26		24.0 ± 0.1, 1.4		Tentative
J123632+621542				<45	<9	<5.9	105 ± 25				
J123702+621009				<45	<9	<5.2	120 ± 27				
J123727+621042				<45	<9	<10.4	220 ± 42				
J123743+621609				<45	<9	<24.0	300 ± 72				

Extensive spectroscopic redshift campaigns have been performed in the HDF-N over the past several years (Cohen et al. 2000; Barger et al. 2000, 2002). An account of available spectroscopic and photometric redshifts was recently presented in Cowie et al. (2004) and Wirth et al. (2004). Unfortunately the overlap with SCUBA counterparts is low, so we are forced to use FIR photometric redshift estimators as well. In Table 5 we provide estimates based on the submillimetre only data, as well as those derived using the Carilli–Yun method (hereafter called the 'CY estimator', Carilli & Yun 1999, 2000) which also employs radio information. As none of the sources are detected at 450 μm, the submillimetre limits are essentially useless, but even with high signal-to-noise ratio detections at 450 and 850 μm, estimating redshifts using FIR SEDs is difficult (Blain, Barnard & Chapman 2003). The CY-estimator is much more constraining.

For the few sources that do have spectroscopic redshifts, the photometric redshifts seem reasonable, although the agreement is far from perfect. The most obvious exceptions are SMMJ123607+621019 and SMMJ123608+621431, which prefer larger redshifts than found by optically based measurements. We already noted that the field around both are quite complex, and lensing may be a factor. However, without confirmation from a CO line detection,

Table 5. Redshift summary of HDF-N submillimetre sources. CY estimates are based on the most likely 1.4-GHz counterpart in the list, or the lower limit in the case of a non-detection. As the CY-estimator is not effective past $z \sim 3$, we cap the lower limits there. The estimates based on ratios between 850- and 450-μm flux densities are listed as well, but only for those cases with $S_{450}/S_{850} < 6.7$, which is the ratio of Arp 220 at redshift zero. $z_{\rm optical}$ is the redshift of the counterpart based on spectroscopy or optical photometry. A question mark is placed in that column if the counterpart has no redshift estimate as yet. Blank entries in this column denote sources where we were unable to determine a counterpart at all.

ID	$z_{\rm CY}$	$z_{450/850}$	$z_{\rm optical}$
850-μm detections $> 4\sigma$			
SMMJ123607+621143	> 3.0	> 0.4	
SMMJ123608+621249	> 3.0	> 0.7	?
SMMJ123616+621516	$2.5^{+1.7}_{-0.8}$	>1.1	2.06[a,b]
SMMJ123618+621007	> 2.9		
SMMJ123618+621552	$1.6^{+0.8}_{-0.4}$	>1.8	?
SMMJ123621+621252	> 3.0		
SMMJ123621+621710	$1.8^{+1.0}_{-0.5}$		?
SMMJ123622+621616	> 3.0	> 0.4	?
SMMJ123634+621407	> 3.0	> 0.3	
SMMJ123637+621155	$3.2^{+2.4}_{-1.2}$	> 0.2	?
SMMJ123645+621449	$1.9^{+1.0}_{-0.5}$	>1.1	?
SMMJ123650+621316	$1.5^{+0.8}_{-0.5}$	>1.1	0.475[c]
SMMJ123652+621225	> 2.7	> 4.9	
SMMJ123656+621201	$2.0^{+1.3}_{-0.6}$	> 2.2	?
SMMJ123700+620910	$1.3^{+1/2}_{-0.4}$		?
SMMJ123701+621146	$1.4^{+0.6}_{-0.4}$		1.52[a,b]
SMMJ123702+621301	> 2.0		
SMMJ123707+621410	$3.7^{+2.8}_{-1.5}$		?
SMMJ123713+621204	> 2.7	> 0.2	
Additional 850-μm detections $> 3.5\sigma$			
SMMJ123607+621019	$3.3^{+5/2}_{-1.2}$		0.47[a,b]
SMMJ123608+621431	$2.1^{+1.4}_{-0.7}$		0.472[c]
SMMJ123611+621213	> 3.0		
SMMJ123628+621046	$1.7^{+0.9}_{-0.5}$		1.013[d]
SMMJ123635+621237	$1.0^{+0.4}_{-0.4}$		1.219[d]
SMMJ123636+620658	> 3.0		
SMMJ123647+621840	> 3.0		
SMMJ123652+621352	>1.5		1.355[d]
SMMJ123653+621119	>1.8		
SMMJ123659+621452	> 2.4		
SMMJ123706+621849	> 3.0		
SMMJ123719+621107	> 3.0		
SMMJ123730+621055	> 3.0		
SMMJ123730+621855	> 3.0		
SMMJ123741+621225	> 3.0		

[a] From Barger et al. (2002).
[b] Redshift determined photometrically from optical counterpart.
[c] From Cowie et al. (2004).
[d] From Barger et al. (2000).

higher-resolution submillimetre data, or further SED information, we are unable to determine whether these are unusual SCUBA galaxies or the wrong identification.

6 CAVEATS TO SOURCE IDENTIFICATIONS

It cannot be stressed strongly enough that the μJy 1.4-GHz radio detections have a high degree of overlap with SCUBA sources, and that they currently constitute the best way to find counterparts to the submillimetre-detected objects. However, there are some cases where the identification still remains ambiguous. HDF 850.1 (SMMJ123652+621225) is a particularly pathological example of how the nearby VLA source may *not* be the correct identification. SMMJ123645+621449 is a case where two radio sources are present near the submillimetre source, and it is difficult to choose which might be the correct identification. Thus the radio-detected submillimetre galaxies that are shaping our understanding of the entire SCUBA population are by no means immune to selection biases. However, it is encouraging that follow-up IRAM observations are detecting CO emission at the redshifts determined via optical spectroscopy (Frayer et al. 1999; Greve, Ivison & Papadopoulos 2003; Neri et al. 2003).

One also has to be aware of two other complications with the identification process – clustering and lensing. As submillimetre galaxies are believed to be associated with merging systems, then it is likely that in many cases the submillimetre bright galaxy will be physically associated *but distinct from* one or more other galaxies which may be submillimetre faint. So one has to be careful when investigating the SEDs, that one is not combining data from multiple objects with very different spectral properties.

Lensing is a further complication, which we know is an important issue for some submillimetre sources in rich cluster fields (Kneib et al. 2004; Borys et al. 2004) and has been suggested for a couple of sources in the HDF region (SMMJ123652+621225 and SMMJ123637+621155). Lensing may make a submillimetre source be apparently associated with a galaxy which actually is in the foreground.

7 SUMMARY AND FUTURE WORK

Concentrating on the more secure ($> 4\sigma$) SCUBA sources, we find that 10 out of 19 have a VLA 1.4-GHz radio counterpart, and at least one more has been radio-detected at a fainter level in a combined map (J123652+6211225, also known as HDF 850.1). This is in line with results from Ivison et al. (2002), Chapman et al. (2002a), Barger et al. (2000) and Greve et al. (2004). This strong overlap, along with the well-determined radio positions, has recently been exploited to obtain redshifts for a large fraction of this subset of sources (Chapman et al. 2003b). However, significant improvements in radio sensitivity are required in order to detect the fainter SCUBA sources, particularly if some of them lie at higher redshifts. Because of this, one cannot simply accept the nearest detected radio source as the correct identification. For example, we argue (see the Appendix) in the case of SMMJ123622+621618 that the radio source 13 arcsec away is *not* responsible for the submillimetre emission (as reported in Barger et al. 2000). Radio sources on their own are not a good way to pre-select SCUBA galaxies, but we note that the subsample of radio detections with $I > 24$ have at least a roughly 30 per cent detection rate in the SCUBA map of HDF-N. This is a lower limit, as much of the submillimetre map is simply too insensitive to sources with $S_{850} \sim 5$ mJy, which is the flux density level where Chapman et al. (2002a) find a much higher (roughly 70 per cent) success rate.

Although X-ray observations help us understand the nature of the SCUBA-detected galaxies, they are not useful in the counterpart identification process in the HDF region. The identification rate is such that the VLA can detect, in a tenth of the time, all the SCUBA galaxies detected by *Chandra*.

There is weak evidence suggesting that the reddest object in the vicinity of a SCUBA source is the correct optical counterpart, but we found no compelling evidence that optical properties alone aid in determining counterparts.

Despite the wealth of deep multiwavelength data in this part of the sky, almost half of our sources have an undetermined counterpart,

clearly demonstrating how difficult it is to make secure identifications. Nevertheless, continued submillimetre imaging in concert with deep *HST* and *Spitzer* data in the region should allow us to characterize the rest-frame UV–NIR spectra of at least the radio-identified galaxies. Confidence in the radio-unidentified half needs to wait for higher-resolution submillimetre images from ALMA. However, in the meantime there is a realistic hope of being able to obtain a full accounting of the submillimetre galaxies in this one small field, and in particular to find out the nature of the currently unidentified half.

ACKNOWLEDGMENTS

We would like to thank Peter Capak, Chuck Steidel, Mark Dickinson, Seb Oliver and Tracy Webb for useful discussions. CB also thanks Ian Smail and Andrew Blain for useful advice on the content and presentation of this paper. We also appreciate advice from the referee which helped streamline the text. This work was supported in part by the Natural Sciences and Engineering Research Council of Canada, as well as by a grant from NASA administered by the American Astronomical Society. The James Clerk Maxwell Telescope is operated by The Joint Astronomy Center on behalf of the Particle Physics and Astronomy Research Council of the United Kingdom, the Netherlands Organization for Scientific Research, and the National Research Council of Canada. Much of the data for this paper was obtained via the Canadian Astronomy Data Centre, which is operated by the Herzberg Institute of Astrophysics, National Research Council of Canada.

REFERENCES

Alexander D. M. et al., 2003a, AJ, 125, 383
Alexander D. M. et al., 2003b, AJ, 126, 539
Almaini O. et al., 2002, in Shanks T., Metcalfe N., eds, ASP Conf. Proc. 283, A New Era Cosmology. Astron. Soc. Pac., San Francisco, p. 377
Almaini O. et al., 2003, MNRAS, 338, 303
Aussel H., Cesarsky C. J., Elbaz D., Starck J. L., 1999, A&A, 342, 313
Barger A. J., Cowie L. L., Richards E. A., 2000, AJ, 119, 2092
Barger A. J., Cowie L. L., Brandt W. N., Capak P., Garmire G. P., Hornschemeier A. E., Steffen A. T., Wehner E. H., 2002, AJ, 124, 1839
Bauer F. E., Alexander D. M., Brandt W. N., Hornschemeier A. E., Vignali C., Garmire G. P., Schneider D. P., 2002, AJ, 124, 2351
Blain A. W., Smail I., Ivison R. J., Kneib J.-P., Frayer D. T., 2002, Phys. Rep., 369, 111
Blain A. W., Barnard V. E., Chapman S. C., 2003, MNRAS, 338, 733
Borys C., Chapman S. C., Halpern M., Scott D., 2002, MNRAS, 330, L63
Borys C., Chapman S., Halpern M., Scott D., 2003, MNRAS, 344, 385 (Paper I)
Borys C. et al., 2004, MNRAS, 352, 759
Capak P. et al., 2004, AJ, 127, 180
Carilli C. L., Yun M. S., 1999, ApJ, 513, L13
Carilli C. L., Yun M. S., 2000, ApJ, 530, 618
Chapman S. C. et al., 2000, MNRAS, 319, 318
Chapman S. C., Richards E. A., Lewis G. F., Wilson G., Barger A. J., 2001a, ApJ, 548, L147
Chapman S., Scott D., Borys C., Halpern M., 2001b, in Lowenthal J. D., Hughes D. H., eds, Deep Millimeter Surveys, World Scientific, Singapore, p. 97
Chapman S. C., Lewis G. F., Scott D., Borys C., Richards E., 2002a, ApJ, 570, 557
Chapman S. C., Shapley A., Steidel C., Windhorst R., 2002b, ApJ, 572, L1
Chapman S. C. et al., 2003a, ApJ, 585, 57
Chapman S. C., Blain A. W., Ivison R. J., Smail I. R., 2003b, Nat, 422, 695
Cohen J. G., Hogg D. W., Blandford R., Cowie L. L., Hu E., Songaila A., Shopbell P., Richberg K., 2000, ApJ, 538, 29
Condon J. J., 1992, ARA&A, 30, 575
Cowie L. L., Barger A. J., Hu E. M., Capak P., Songaila A. 2004, AJ, 127, 3137
de Ruiter H. R., Arp H. C., Willia A. G., 1977, A&AS, 28, 211
Désert F.-X., Puget J.-L., Clements D. L., Pérault M., Abergel A., Bernard J.-P., Cesarsky C. J., 1999, A&A, 342, 363
Downes A. J. B., Peacock J. A., Savage A., Carrie D. R., 1986, MNRAS, 218, 31
Downes D. et al., 1999, A&A, 347, 809
Dunlop J. S. et al., 2004, MNRAS, 350, 769
Eales S., Lilly S., Gear W., Dunne L., Bond J. R., Hammer F., Le Fèvre O., Crampton D., 1999, ApJ, 515, 518
Farrah D., Afonso J., Efstathiou A., Rowan-Robinson M., Fox M., Clements D., 2003, MNRAS, 343, 585
Ferguson H., Dickinson M., Williams R., 2000, ARA&A, 38, 667
Fixsen D. J., Dwek E., Mather J. C., Bennett C. L., Shafer R. A., 1998, ApJ, 508, 123
Frayer D. T. et al., 1999, ApJ, 514, L13
Garrett M. A., de Bruyn A. G., Giroletti M., Baan W. A., Schilizzi R. T., 2000, A&A, 361, L41
Goldschmidt P. et al., 1997, MNRAS, 289, 465
Greve T. R., Ivison R. J., Papadopoulos P. P., 2003, ApJ, 599, 839
Greve T. R., Ivison R. J., Bertoldi F., Stevens J. A., Dunlop J. S., Lutz D., Carilli C. L., 2004, MNRAS, in press (doi: 10.1111/j.1365-2966.2004.08235.x) (astro-ph/0405361)
Hamilton A. J. S., 1993, ApJ, 417, 19
Hauser M. G. et al., 1998, ApJ, 508, 25
Holland W. S. et al., 1999, MNRAS, 303, 659
Hughes D. H. et al., 1998, Nat, 394, 241
Ivison R. J. et al., 2002, MNRAS, 337, 1
Johnstone D., Wilson C. D., Moriarty-Schieven G., Giannakopoulou-Creighton J., Gregersen E., 2000, ApJS, 131, 505
Kneib J., van der Werf P. P., Kraiberg Knudsen K., Smail I., Blain A., Frayer D., Barnard V., Ivison R., 2004, MNRAS, 349, 1211
Mendez R. A., Guzman R., 1998, A&A, 333, 106
Mohan N. R., Cimatti A., Röttgering H. J. A., Andreani P., Severgnini P., Tilanus R. P. J., Carilli C. L., Stanford S. A., 2002, A&A, 383, 440
Nandra K., Mushotzky R. F., Arnaud K., Steidel C. C., Adelberger K. L., Gardner J. P., Teplitz H. I., Windhorst R. A., 2002, ApJ, 576, 625
Neri R. et al., 2003, ApJ, 597, L113
Nousek J. A., Garmire G. P., Ricker G. R., Collins S. A., Reigler G. R., 1987, ApL, 26, 35
Peacock J. A. et al., 2000, MNRAS, 318, 535
Prestage R. M., Peacock J. A., 1983, MNRAS, 204, 355
Puget J.-L., Abergel A., Bernard J.-P., Boulanger F., Burton W. B., Desert F.-X., Hartmann D., 1996, A&A, 308, L5
Richards E. A., 2000, ApJ, 533, 611
Richards E. A., Kellermann K. I., Fomalont E. B., Windhorst R. A., Partridge R. B., 1998, AJ, 116, 1039
Scott D., Tout C. A., 1989, MNRAS, 241, 109
Scott S. E. et al., 2002, MNRAS, 331, 817
Serjeant S. et al., 2003, MNRAS, 344, 887
Shapley A., Fabbiano G., Eskridge P. B., 2001, ApJS, 137, 139
Steidel C. C., Adelberger K. L., Dickinson M., Giavalisco M., Pettini M., Kellogg M., 1998, ApJ, 492, 428
Steidel C. C., Adelberger K. L., Shapley A. E., Pettini M., Dickinson M., Giavalisco M., 2003, ApJ, 592, 728
Stocke J. T., Morris S. L., Gioia I. M., Maccacaro T., Schild R., Wolter A., Fleming T. A., Patrick H. J., 1991, ApJS, 76, 813
Wang W.-H., Cowie L., Barger A., 2004, ApJ, in press (astro-ph/0409087)
Webb T. M. A., Sawicki M., 2004, ApJ, in press (astro-ph/0402454)
Webb T. M. et al., 2003a, ApJ, 582, 6
Webb T. M. A., Lilly S. J., Clements D. L., Eales S., Yun M., Brodwin M., Dunne L., Gear W. K., 2003b, ApJ, 597, 680
Webb T. M. A., Brodwin M., Eales S., Lilly S. J., 2004, ApJ, 605, 645
Wehner E. H., Barger A. J., Kneib J.-P., 2002, ApJ, 577, L83
Williams R. E. et al., 1996, AJ, 112, 1335
Wirth G. D. et al., 2004, AJ, 127, 3121

APPENDIX A: MULTIWAVELENGTH DESCRIPTION OF SUBMILLIMETRE-DETECTED SOURCES IN GOODS-N

A1 850-μm sources from the primary catalogue

Here we describe the 19 objects in the 4σ HDF-N SCUBA catalogue. We name the objects according to their positions and using the 'SMMJ' prefix, which has become conventional. In square brackets we use the letters J, S and P to indicate that the data were collected by jiggle-map scan-map or photometry observations, respectively. All optical magnitudes are given in the AB system. The 19 strips of postage stamps are shown in Fig. A1, and some of the collected photometry can be found in Tables 2 and 4.

SMMJ123607+621143 [S]. A weak radio source detected by WSRT lies 8 arcsec to the east. An inspection of the VLA map shows a 4σ peak near this position, although it is 2 arcsec even further east from the SCUBA galaxy (but consistent with the offset between the catalogues as discussed previously). Interestingly, the weak VLA source is coincident with a red ($R - HK' = 3.3$) galaxy. Given the rarity of such sources, it is tempting to associate the submillimetre galaxy with it, despite the offset. However, this is well outside our 7-arcsec search radius, so we dismiss it. There are five optically detected objects within the search area but with no further information we cannot assign a robust counterpart to this source.

SMMJ123608+621249 [S]. This source lies directly on top of a very faint object ($R = 25.2 \pm 0.1$). There are no other optical counterparts within 7 arcsec, and no radio or X-ray objects anywhere near the SCUBA source, thus suggesting this as the tentative identification.

SMMJ123616+621516 [JS]. two radio sources are found within 7 arcsec, one from the WSRT and one from the VLA. These are not spatially coincident, but given that the fluxes are comparable, and the WSRT position is west of the VLA source (again consistent with the offset between the catalogues), they are likely to be the same source. The optical counterpart is fairly faint, and appears to have a faint red companion 1 arcsec to the north-west. Coincident with the radio identification is a blended *Chandra* source. Note that this object is discussed in some detail in Alexander et al. (2003a). They describe the second X-ray source as invisible in the radio and optical bands, and though not formally detected, the postage stamps do suggest that the second object is red and radio faint. We choose the radio-detected X-ray source as the identification, though point out that the submillimetre flux may be due to the much fainter optically detected galaxy or a combination of both.

SMMJ123618+621007 [JS]. The VLA source (detected in X-ray and optical images) 13 arcsec away is too far to comfortably call it the counterpart. Within 20 arcsec there are three LBGs, but the closest is 8.3 arcsec away. As we find two optically detected galaxies within 6 arcsec, we cannot assign an identification. We note an even fainter galaxy which, although not in the $> 5\sigma$ optical catalogue, is seen in the optical thumb-nails and seems to lie directly on the SCUBA centroid.

SMMJ123618+621552 [JS]. A strong 1.4-GHz VLA source (151 μJy) with a very steep spectrum lies 3.5 arcsec to the south-west. An 8.5-GHz source is also seen there, though not formally listed in the catalogue. We consider this radio source to be the counterpart. The only optically detected galaxy in the search region is a faint optical source 2 arcsec north of the VLA position, but a fainter (and formally undetected) HK' source is coincident with the radio range.

SMMJ123621+621252 [JS]. Two optically detected galaxies are present within the search area, meaning we cannot assign a robust identification. Outside of the 7-arcsec search radius, the field is rather dense with optically detected galaxies. There are also seven *Chandra* sources in total within 18 arcsec of the SCUBA source.

SMMJ123621+621710 [JS]. An extended radio source is coincident with the SCUBA position. Its north-western end is coincident with an optically detected galaxy that has an elongated morphology perpendicular to the radio extension. Although not listed in the 2-Ms *Chandra* catalogue, there is extended soft X-ray emission clearly seen. We use this VLA source as the SCUBA counterpart.

SMMJ123622+621616 [JS]. Barger et al. (2000) associates this object with the radio source 13 arcsec to the north. This is well outside our search radius, however, and we do not assign it as the correct identification. Alexander et al. (2003a) use this object as a possible example of a Compton-thick AGN, but they noted the inferred redshift ($z = 0.46^{+0.03}_{-0.02}$), based on a 2.3σ iron line in the X-ray spectrum, was considerably different from that obtained via fits to the FIR-radio SED of the galaxy ($z = 2.4^{+1.1}_{-0.8}$). In the optical catalogues, there is a pair of galaxies separated by less than 1 arcsec and three other objects within the 7-arcsec search radius.

SMMJ123634+621407 [JS]. Although the field is dense in optically detected sources, one unique object in the vicinity is an X-ray-detected LBG with $z = 3.408$. The 11.4-arcsec offset is rather large, especially considering the 850-μm flux density is well above the confusion level and the SNR is high. The ISO 15-μm detection 5.3 arcsec to the south is the more appealing counterpart, and there is an 8.5-GHz object coincident with the *ISO* centroid. However, it is not listed in the 8.5-GHz catalogue, and no 1.4 GHz or optical flux is detected here. We conclude that there is no robust counterpart.

SMMJ123637+621155 [JSP]. A 4σ radio detection by the WSRT (but not VLA) does not appear coincident with any other object, but the VLA map does reveal radio flux, though not quite at the same position. Seemingly unrelated are two optical candidates, which both have spectroscopic redshifts, and lie within 4 arcsec of the SCUBA source. The first is a $z = 0.779$ galaxy with $R = 22.5$, $R - HK' = 1.6$. The second is a $z = 0.557$ galaxy with $R = 22.4$, $R - HK' = 1.6$, which also happens to line up with a soft X-ray source. At these redshifts it is difficult to understand the lack of a radio detection if one of these two objects were the SCUBA counterpart. As explained in Section 4.2.3, we suggest that these optically detected galaxies are lensing the SCUBA source, and that the radio object is the true identification.

SMMJ123645+621449 [SP]. There are two 1.4-GHz VLA sources coincident with *Chandra* detections near the SCUBA source, and we choose the one closest to the SCUBA centroid (also the brighter of the two). This object is also detected at 8.5 GHz. The other radio source is detected by *ISO*. Redshifts would be useful for determining if the radio pair is indeed spatially related.

SMMJ123650+621316 [JSP]. The counterpart that meets our criterion is detected in most wavebands – both radio frequencies,

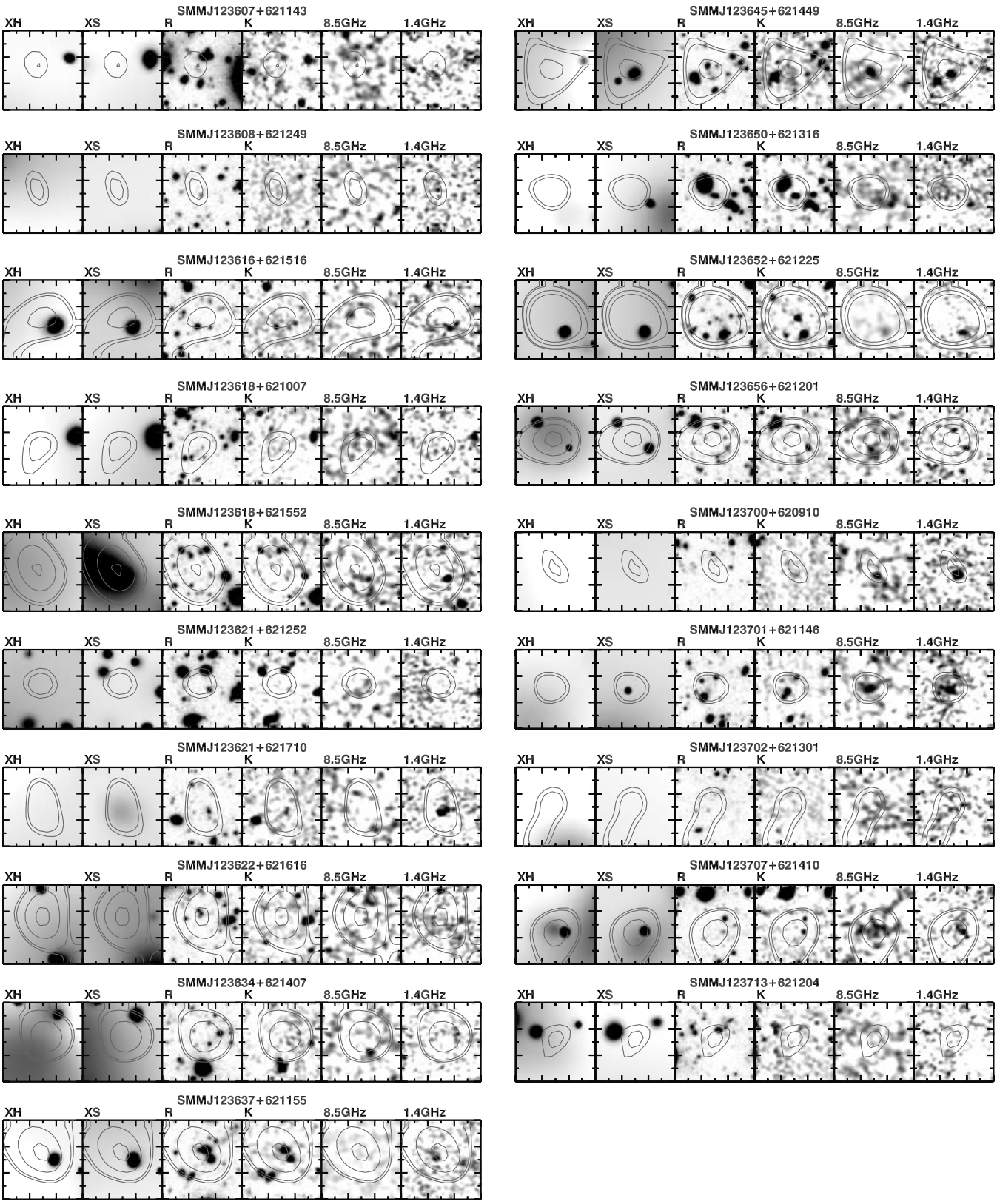

Figure A1. Postage stamps of the $> 4\sigma$ 850-μm SCUBA sources showing: XH (hard X-ray); XS (soft X-ray); *R* and *HK′* (ground-based optical imaging); 8.5 and 1.4 GHz (VLA radio). These data are described in Section 4. We show 30 arcsec on a side negative images at each waveband, with north and east running towards the top and left of the page, respectively. 3.5, 4, 6 and 8σ SCUBA 850-μm contours are overplotted on each.

15 μm, X-ray and optical bands, and also has a redshift of 0.475. The faintness of this submillimetre source suggests that confusion noise may be a particular problem, but if the radio flux is coming from the SCUBA source, then the radio/submillimetre flux density ratio is a factor of 10 too low for this redshift. Note that this SCUBA source is considered as two distinct objects (HDF 850.4/HDF 850.5) by Serjeant et al. (2003), but the combined submillimetre data that make up the Super-map yield only a single source. As its profile is quite Gaussian, we do not treat the possibility of it being two sources.

SMMJ123652+621225 [JSP]. This object (also known as HDF850.1) is discussed at length in Section 5.2.

SMMJ123656+621201 [JSP]. This SCUBA object is commonly called HDF 850.2, and at only 3.7 mJy, has a position that may be affected by confusion noise. The faint radio source 5.8 arcsec to the north seems like the correct identification, but has no optical counterpart. We note that there is a pair of LBGs just to the south-west, one of which is *Chandra*-detected and has radio emission just below the VLA catalogues' threshold. The LBG was discussed by Nandra et al. (2002), who noted that if at redshift 3, this galaxy is almost certainly an AGN, given its X-ray luminosity. If at the same redshift, the small separation of the LBGs suggests they are interacting, which makes it an appealing choice for the SCUBA counterpart. Another mark in its favour is that the submillimetre flux density is very small, which would be in line with the rare submillimetre detections of LBGs. Although the LBGs are the more interesting case, our counterpart criterion favours the faint radio-detected object.

SMMJ123700+620910 [JS]. The only obvious contender is an optically invisible radio source (detected by the VLA at both frequencies) only a few arcsec away from the SCUBA position.

SMMJ123701+621146 [JS]. Directly on top of the SCUBA centroid is a striking radio and X-ray-detected ERO. The object 2 arcsec to the south-east of the ERO has a redshift of 0.884 and an *ISO* 15-μm detection. However, it is possible that the *ISO* flux is actually coming from the ERO. Given the proximity of the source, the ERO may well be lensed by the foreground ($z = 0.884$) galaxy.

SMMJ123702+621301 [JSP]. The elongated contours suggest the blending of two nearby sources. The lower part does seem to be centred on an optically detected galaxy. However, we find no convincing counterpart to the SCUBA source.

SMMJ123707+621410 [JSP]. The correct identification seems highly likely to be the optically red radio and X-ray-detected object right on top of the SCUBA source.

SMMJ123713+621204 [JS]. There are no radio, red objects or X-ray sources nearby that are convincing enough to call a counterpart. Two galaxies in the *R*-selected catalogue fall within 7 arcsec, but we are unable to determine which (if either) is the correct identification.

A2 850-μm sources from the supplementary catalogue

In this subsection we describe the 15 objects in the supplementary HDF-N SCUBA catalogue of sources detected with a SNR between 3.5σ and 4σ. The postage stamps are shown in Fig. A2.

SMMJ123607+621019 [S]. A *Chandra* detected radio galaxy seems the obvious identification, although the radio/submillimetre flux density ratio is too low for the redshift of 0.47 (determined from optical photometry). The optical emission suggests a disturbed system, and the surrounding area is very dense with galaxies. Indeed, Barger et al. (2002) note that the photometric redshift may be contaminated by flux from neighbouring galaxies.

SMMJ123608+621431 [JS]. The identification is likely to be the X-ray and radio-detected object to the north.

SMMJ123611+621213 [S]. The radio map shows a 4σ source 4 arcsec east of the SCUBA position, but with no optical counterpart. Although deeper observations may confirm this radio identification, for now we conclude that there is no counterpart.

SMMJ123628+621046 [JS]. The $z = 1.013$ very red object that has detections in the optical, radio and X-ray is the counterpart.

SMMJ123635+621237 [JSP]. This faint submillimetre source is HDF 850.7 in the Serjeant et al. (2003) catalogue. It lies in a complex field, with the most appealing candidate being a $z = 1.219$ red galaxy. This has detections in the radio, mid-IR and X-ray. Unfortunately this candidate lies 7.6 arcsec to the west of the SCUBA centre, but again this may be due to confusion noise. The redshift is compatible with that derived from the CY estimator. Despite the slightly large offset, we will select this as the counterpart.

SMMJ123636+620658 [S]. There is a very bright (presumably foreground) galaxy with radio emission to the north. A fainter source next to it appears distorted (and perhaps redder). From this fainter object there is radio emission and hard X-ray flux. However, this radio source is distant (over 11 arcsec away), and submillimetre confusion is not a big issue here, as the source is so bright. We therefore conclude there is no counterpart.

SMMJ123647+621840 [S]. This is also scan-map only (like the previous source), but near the northern edge of the map. It is apparently a blank field to the limit of the observations

SMMJ123652+621352 [JSP]. Three moderate redshift *ISO* objects are within 11 arcsec, but the SCUBA centre lies on top of a non-ISO-detected $z = 1.355$ galaxy that also has *Chandra* and 8.5-GHz detections. This is the only case where we base the radio identification on the 8.5-GHz data rather than that at 1.4 GHz. Serjeant et al. (2003) note that this source (HDF 850.8) is part of an interacting pair of galaxies.

SMMJ123653+621119 [SP]. There are too many optically detected sources present to choose from. The nearby soft X-ray source does not have any detectable radio flux, but is present in the X-ray study of star-forming galaxies by Nandra et al. (2002). This Balmer break galaxy has a redshift of 0.89 and an inferred SFR of $30\,M_{\odot}\,yr^{-1}$. The small submillimetre flux density is still moderately high for this SFR, and without a radio detection we can only speculate that this is the correct identification.

SMMJ123659+621452 [SP]. 7 arcsec to the south-east is a $z = 0.762$ X-ray, 1.4-GHz radio- and *ISO*-detected object. 7 arcsec to the west lies a $z = 0.849$ 8.5-GHz radio- and *ISO*-detected object. This latter object also has a faint 1.4-GHz flux. Both objects have very

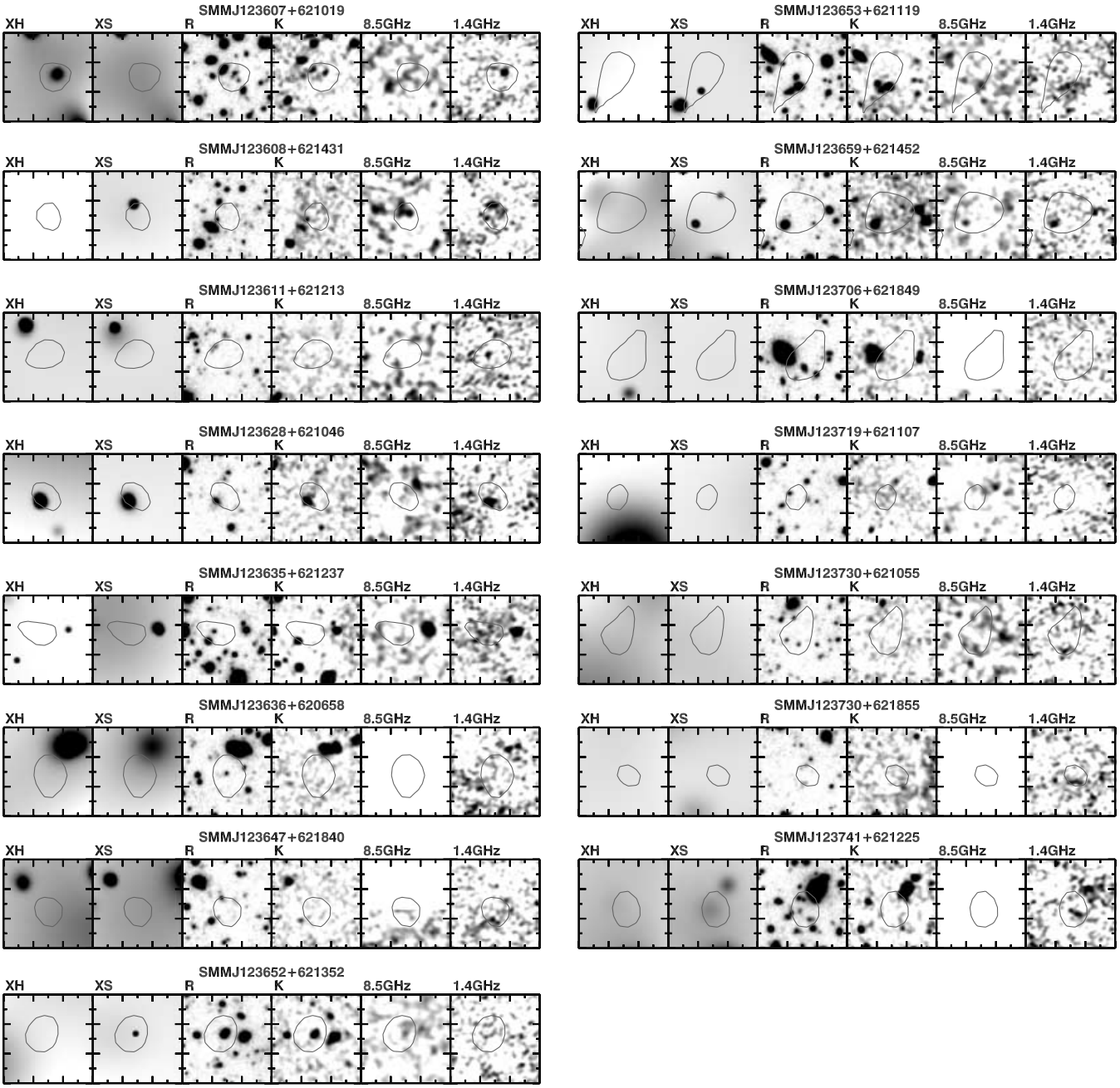

Figure A2. Postage stamps of the 3.5σ < SNR < 4.0σ 850-μm SCUBA sources. These are the 17 sources from this supplementary catalogue. The images are as described in Fig. A1.

similar radio and 15-μm fluxes, and hence both predict a similar redshift when using the 850-μm fluxes as a photometric redshift indicator.

SMMJ123706+621849 [S]. It is difficult to choose among the three (at least) optical sources in the region, especially in the absence of any other multiwavelength data. Note the extended soft X-ray flux overlapping the 850-μm contours.

SMMJ123719+621107 [JS]. There are four optically detected galaxies within 7 arcsec of the SCUBA position, none of which have a radio detection that can be used to help discern if any are the SCUBA counterpart.

SMMJ123730+621055 [S]. No obvious counterpart.

SMMJ123731+621855 [S]. No obvious counterpart.

SMMJ123741+621225 [S]. There is a radio source 7.6 arcsec to the north. It overlaps with soft X-ray flux as seen in the *Chandra* image, although it is not formally listed in the Alexander et al. (2003) *Chandra* catalogue. The SCUBA contours prefer a very faint galaxy pair which appears to have some radio flux.

A3 450–μm detections >3.5σ

We now describe the five objects in the HDF-N SCUBA map that were detected at > 4σ confidence at 450 μm. Here we search for

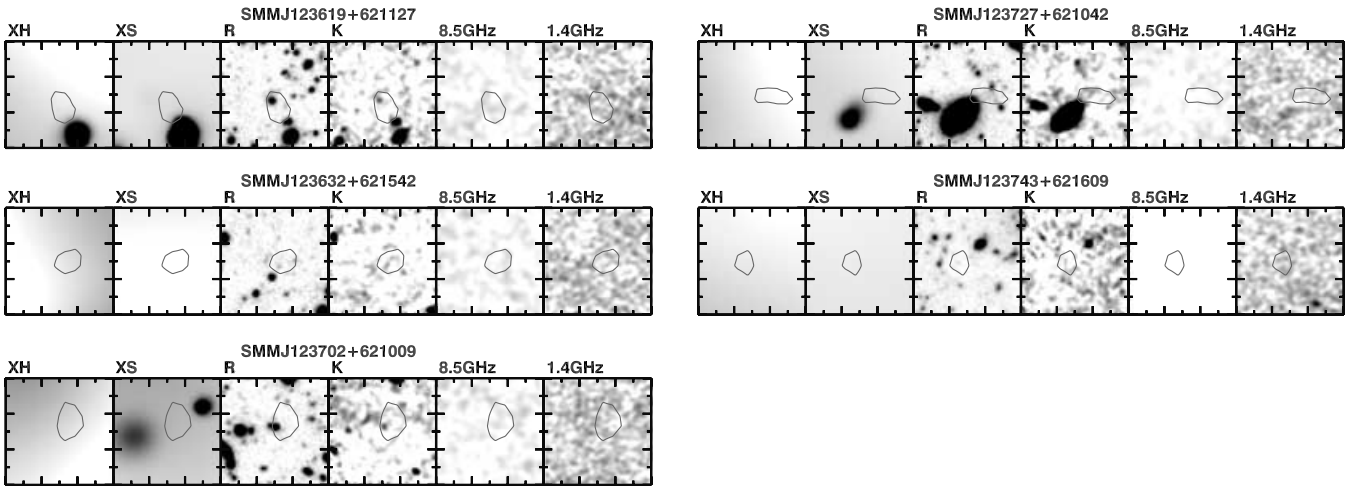

Figure A3. Postage stamps of the $> 4\sigma$ 450-μm SCUBA objects.

counterparts within 4 arcsec of the SCUBA centroid. Although the beam-size is smaller at 450 μm (7.5 arcsec), the search radius still needs to be reasonably large, because of the other systematic effects described in Section 3. It is also worth noting that anything detected at 450 μm should have been seen at 850 μm, unless the source has an extremely steep emissivity ($\beta > 3.5$). We are much less confident concerning the reliability of our 450-μm candidates, but nevertheless present them for completeness (see also Fig. A3).

SMMJ123619+621127 [JS]. As there is only one optically detected galaxy within the search radius, we assign it as the tentative identification.

SMMJ123632+621542 [JS]. No obvious counterpart.

SMMJ123702+621009 [JS]. Two optical galaxies relatively near to the centroid make it impossible to tell which is the counterpart.

SMMJ123727+621042 [S]. A large elliptical galaxy is nearby, but still too far to have it be the unambiguous identification.

SMMJ123743+621609 [S]. No obvious counterpart

APPENDIX B: OTHER INTERPRETATIONS

Using existing and new submillimetre data, Wang et al. (2004) have recently presented another SCUBA map of the HDF-N. They provided a catalogue of 17 $> 4\sigma$ objects,[1] as well as several more between 3 and 4σ. Given the strong interest in the GOODS-N region by many in the community, we briefly discuss the similarities and differences between the different analyses.

B1 Source catalogues

Ignoring three Super-map sources that were found in regions sampled mainly in the scan-map mode, we find that 14 of 16 4σ Super-map sources are recovered in the list provided by Wang et al. (2004). SMMJ123701+621146 (also known as HDF850.6) and SMMJ123702+621301 are not detected in their list because they use less data and are hence less sensitive. A full comparison is presented in Table B1.

Of their 17 4σ objects, 14 are already detected in our 4σ catalogue. Of the missing three, GOODS850-06 is in a region where the Super-map has low sensitivity (which they supplemented with deeper jiggle-maps), another (GOODS850-17) is detected in our catalogue at just under 4σ, and the final object (GOODS850-08) is in a suspicious region that we address shortly. It is encouraging that separate groups can reproduce similar sources using different techniques. We do note that the correlation between sources detected under 4σ is much weaker, but one would expect this given the poor reliability of low signal-to-noise ratio sources.

Table B1. Comparison between sources in Paper I and those reported in Wang et al. (2004). Here we compare the fluxes and offsets between sources in our Super-map (B03), and those in Wang et al. (2004). Some scan-map sources are discrepant, but see the text for an explanation.

ID		θ	S850 (mJy)	
B03	W04	(arcsec)	B03	W04
J123607+621143	31	18	15.2 ± 3.9	4.4 ± 1.3^a
J123608+621249	40	10	16.0 ± 3.7	3.9 ± 1.3^a
J123616+621516	07	4	6.1 ± 0.9	6.2 ± 1.0
J123618+621007	24	4	6.6 ± 1.5	6.0 ± 1.7
J123618+621552	03	1	7.2 ± 0.9	7.7 ± 1.0
J123621+621252	14	26	12.1 ± 2.6	10.5 ± 2.3^a
J123621+621710	15	2	8.8 ± 1.5	8.7 ± 2.0
J123622+621616	02	5	8.6 ± 1.0	10.3 ± 1.2
J123634+621407	05	6	11.2 ± 1.6	12.9 ± 2.1
J123637+621155	04	13	7.0 ± 0.8	8.6 ± 1.3
J123645+621449	11	1	8.5 ± 1.3	10.8 ± 2.2
J123650+621316	10	5	2.9 ± 0.4	2.6 ± 0.5
J123652+621225	01	1	5.9 ± 0.3	5.1 ± 0.5
J123656+621201	12	0	3.7 ± 0.4	3.3 ± 0.7
J123700+620910	16	5	8.6 ± 2.1	12.4 ± 2.9
J123707+621410	09	7	9.9 ± 2.5	7.0 ± 1.2
J123713+621204	13	2	6.1 ± 1.4	7.0 ± 1.5

[a] Scan-map sources.

[1] Wang et al. (2004) label their objects GOODS850-01 through GOODS850-17, while we use the prefix SMMJ combined with the coordinates of the object

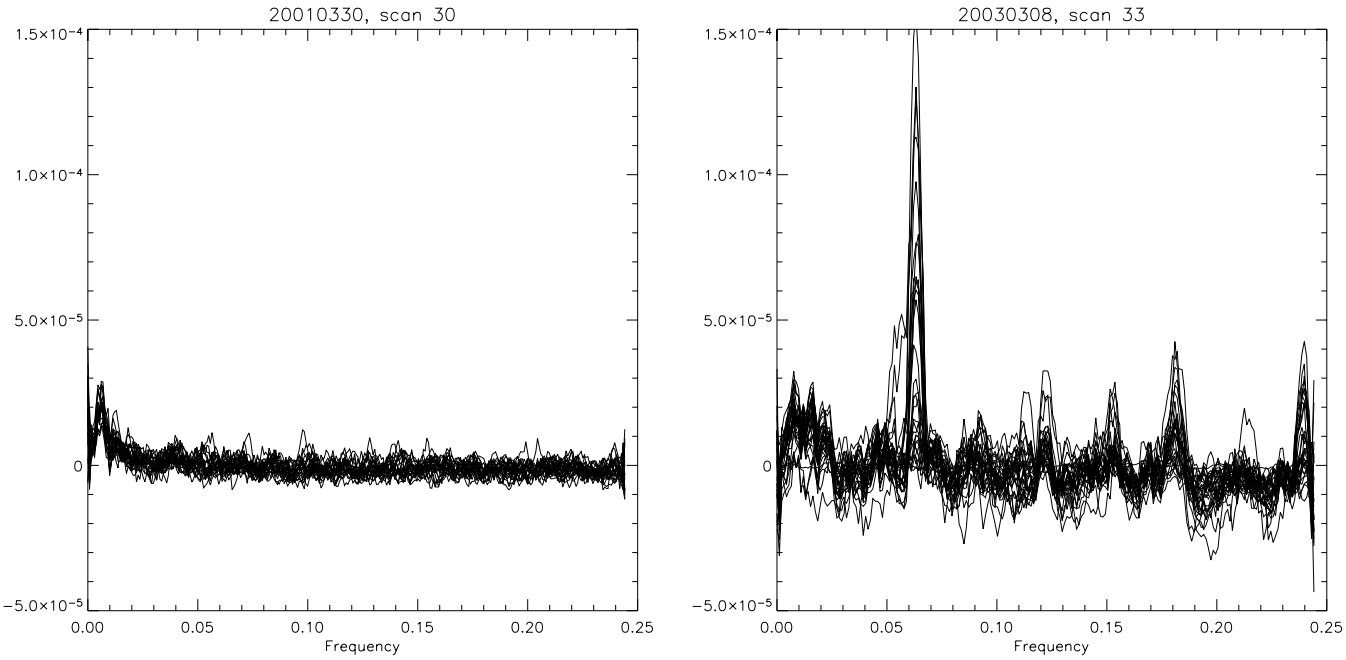

Figure B1. The scan-synchronous noise glitch. The left-hand panel shows data taken while SCUBA was stable. It is a collection of power spectra taken from all bolometers, which is calculated using Fourier transforms of the raw data. We label the abscissa 'Frequency', although it is in fact the Fourier conjugate of the sample number. Samples are collections of chopped data taken 16 s apart (this is how SCUBA records data). The right-hand panel clearly shows more insipid power spectra, especially at a period of 16 samples. This corresponds to the same period on which the 16-point dither pattern operates, meaning noise can be projected on to the map at regular positions.

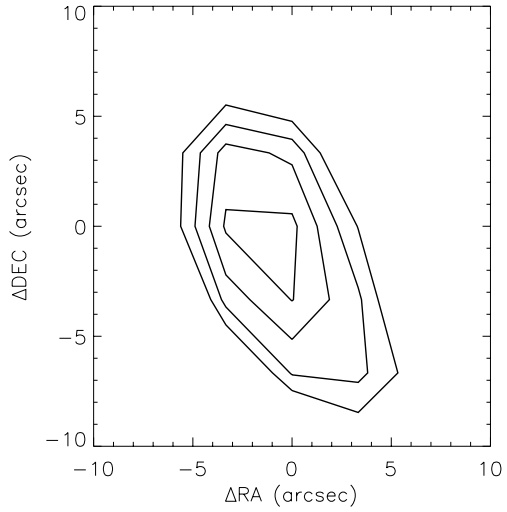

Figure B2. Cross-correlation of maps made from scan and jiggle data separately. Contours are plotted at 1, 2, 3 and 4σ. These were calculated using pixels within 6 arcsec of all objects in the final 4σ catalogue, and demonstrate a very strong correlation between the two maps.

B2 Jiggle-map 'noise-spike'

The only significant differences seem to be around SMMJ123607+621143 and SMMJ123608+62124, which were first detected in the scan-map of Borys et al. (2002). Wang et al. (2004) claim scan-map data are suspect as they fail to recover them in new jiggle-map data. Their source catalogue contains three objects between 3.0 and 3.5σ, two more between 3.5 and 4.0σ, and one $> 4\sigma$ within a SCUBA array size centred on these sources. This is an unusually large number for a typical 'blank field' SCUBA observation,[2] and none of them have a plausible radio counterpart, nor are coincident with any of the scan-map sources.

We believe some of the discrepancy arises due to the 'noise-spike' issue discovered by one of us (Borys) in jiggle-map observations taken around the same time[3] (see Fig. B1). This instrumental fault has manifested itself in the map published in Webb & Sawicki (2004), as well as in data from the SHADES survey (J. Dunlop, private communication). Roughly two-thirds of the array is affected (24 bolometers) by noise that is scan-synchronous, i.e. the noise-spike occurs at the same frequency as the dither pattern cycle that makes up the jiggle-map. Therefore, the noise is projected into discrete places on the sky, and does not integrate down as $t^{-1/2}$. Though it is known that the problem affects source fluxes and increases the number false positives, there is currently no proven algorithm which removes this. Wang et al. (2004) note their data are affected by this issue and removed a small number of especially noisy bolometers. Our own research has shown that this may not be sufficient, as during the sky subtraction phase of the data reduction, the bolometers affected by the noise corrupt the bolometers which are not. Fixes are being developed by our own group, the SHADES team (A. Mortier private communication), and T. Webb (private communication). IDL based code to identify the data affected by this issue is available from the author by request.

Still, it useful to check to see how consistent scan-map and jiggle-map data are. As described in Paper I, we cross-correlated the jiggle and scan-maps in order to check the relative calibration and pointing offsets (none of the 'corrupt' jiggle-map data were used). Fig. B2

[2]The number counts at this flux level suggest there should be at most two $> 3\sigma$ sources in an area the size of the SCUBA array.

[3]Semesters 02B and 03A seem particularly affected, the problem was noted in other semesters to varying degrees as well.

verifies that the two maps are sensitive to the same sources. Given the success in using the scan-map mode for other projects (e.g. Johnstone et al. 2000), there is no a priori reason to suspect that the scan-map technique is not viable. It is likely that a resolution between the recent results in Wang et al. (2004) and our Super-map will require new observations from a well characterized and healthy submillimetre instrument. Nevertheless, we stress that aside from this one region, the final source catalogues in Wang et al. (2004). and Paper I are very consistent.

B3 Multiwavelength identifications

Regarding the multiwavelength identifications, Wang et al. (2004) find a similar radio association rate. Though by including HDF850.1 (SMMJ123652+621225) and SMMJ123622+621616 (which is uncomfortably far away from the nearest radio source), they have estimated a higher radio-identification fraction than we found with our more rigorous identification recipe. However, the most significant difference between the multiwavelength identifications is that Wang et al. (2004) use X-ray or *ISO*-detected objects that have no radio counterpart to tag some SCUBA objects. As we have demonstrated in this paper, unless there is a believable radio source as the counterpart, we find no convincing evidence that an association can be made with another wavelength.

This paper has been typeset from a TEX/LATEX file prepared by the author.